NON EQUILIBRIUM DYNAMICS OF QUANTUM ISING CHAINS IN THE PRESENCE OF TRANSVERSE AND LONGITUDINAL MAGNETIC FIELDS

by

Zahra Mokhtari

THESIS SUBMITTED IN PARTIAL FULFILLMENT

OF THE REQUIREMENTS FOR THE DEGREE OF

MASTER OF SCIENCE

IN THE

DEPARTMENT OF PHYSICS

FACULTY OF SCIENCE

SIMON FRASER UNIVERSITY

Summer 2013

APPROVAL

Name: Zahra Mokhtari

Degree: Master of Science

Title of Thesis: Non equilibrium dynamics of quantum Ising chains in the presence of transverse and longitudinal magnetic fields

Examining Committee: Dr. J. Steven Dodge, Associate Professor (Chair)

Dr. Malcolm P. Kennett, Senior Supervisor
Associate Professor

Dr. Paul C. Haljan, Supervisor
Associate Professor

Dr. George Kirczenow, Supervisor
Professor

Dr. Eldon Emberly, Internal Examiner
Associate Professor

Date Approved: August 26, 2013

Partial Copyright Licence

Abstract

There has been much recent interest in the study of out of equilibrium quantum systems due to experimental advances in trapped cold atomic gases that allow systematic studies of these effects. In this work we study a quantum Ising model in the presence of transverse and longitudinal magnetic fields. The model lacks an analytical solution in the most general case and has to be treated numerically. We first investigate the static properties of the model, including the ground state energy and the zero temperature phase diagram, using the Density Matrix Renormalization Group (DMRG) method. We identify ordered and disordered phases separated by a quantum phase transition. We then consider the time evolution of the system following an abrupt quench of the fields. We study the response of the order parameter to the quenches within the ordered and disordered phases as well as quenches between the phases using the time-dependent DMRG method. The results are in qualitative agreement with experiments and the implemented numerical method in this work can be extended to allow for more general interactions.

Acknowledgments

My gratitude extends to many people, the preciousness of whom a thank-you will hardly acknowledge.

I would like to thank my supervisor, Dr. Malcolm Kennett, whose constant support and hope in the most disappointing situations, his helpful guidance, and endless energy were all new and very invaluable to me.

I like to thank my friends, Matthew, Fatemeh, Dorna, Peter, Saeed, and Zahra, without whom I would not have enjoyed my two-year life in Vancouver the same way. And Rose and Stephen, for their all-time help. I owe special thanks to my roommates here: Elizabeth and Homa. They have indeed been like my temporary family and have always been kind to me even in my busy and messy days.

My deepest gratitude goes to my family, mom, dad, Elaheh, and my love, Ehsan. I had no idea how sad and pointless my life would be without them when I was leaving, but they never really left me. And this whole work would be far from complete without their unique support.

Contents

List of Figures

Chapter 1

Introduction

Spin, the intrinsic angular momentum of quantum particles, was discovered by Stern and Gerlach in 1922 [1]. It was realized shortly afterwards [2] that the magnetic properties of materials involve the co-operative interactions of electron spins in solids. This initiated the study of models of quantum spins with the goal of describing magnetic materials. One of the very basic questions to answer is how to relate the macroscopic magnetic properties of materials to interactions at the microscopic scale. Hence, one strand of research in this field has involved the study of idealized models, each describing a particular class of interactions, to further understanding of the macroscopic behaviour from different microscopic interactions.

In 1925 the one dimensional Ising model was introduced [3] and found to exhibit no phase transition and hence no magnetic ordering at finite temperature. The two dimensional Ising model was not solved exactly until 1944 [4] when it was shown to exhibit a magnetically ordered phase below a critical temperature. An early important result was obtained in 1931 when Bethe introduced an exact solution for finding the eigenvalues and eigenvectors of the spin $\frac{1}{2}$ Heisenberg model on a chain [5], which was used by Hulthen [6] to compute the ground state energy of the antiferromagnetic spin $\frac{1}{2}$ Heisenberg chain and was later extended to other models [7]. In 1961, Lieb *et al.* [8] exactly solved the XY and Heisenberg-Ising models of antiferromagnetic chains by mapping the spins in these problems to spinless fermions via the Jordan Wigner transformation, and investigated the existence of long-range order in such models. Studies of the Ising model in a transverse field in 1960s [9] have had a strong contribution to the understanding of quantum phase transitions at zero temperature, since this model exhibits a quantum phase transition and has an analytical solution which allows for the exact calculation of observables (this will be discussed in Chapter 2).

In recent years, understanding the collective behaviour of quantum mechanical systems of many particles has become an important topic of research, particularly with the prospect of applications in quantum computing and quantum information. Quantum phase transitions between magnetically ordered and disordered phases are one class of such phenomena. At zero temperature, interactions can give rise to collective behaviours such as spontaneous alignment of all the spins in a particular direction (spontaneous magnetization), i.e. indicating a transition from a magnetically disordered to ordered phase. Quantum phase transitions are distinct from the classical ones in the nature of the fluctuations that leads to the transition. Instead of thermal fluctuations at finite temperature in classical phase transitions, at zero temperature quantum fluctuations give rise to a nonanalyticity in the ground state energy of the system.

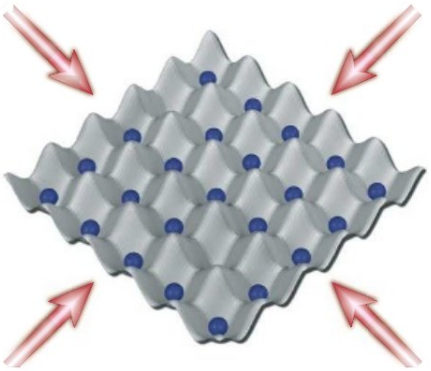

Figure 1.1: Two-dimensional optical lattice formed by superposition of two standing waves [10].

Experimental studies in this field in solid state systems can be challenging due to the macroscopic number of degrees of freedom, disorder, unknown interactions, and limitations on which system parameters can be varied [11]. An experimental setting in which system parameters can be controlled very well is trapped cold atoms (and also trapped ions), which provides exciting possibilities for quantum simulations [12]. In cold atom experiments, neutral atoms can be cooled and trapped in optical lattices due to the interaction between their induced dipole and the electric field associated with the lattice [13]. Optical lattices, light-induced periodic potentials created by the interference pattern of counter propagating laser beams (Figure 1.1) offer the possibility of tuning system parameters, such as lattice depth and structure, dimensionality, and the interactions with high precision. Therefore cold atom experiments in which quantum spins are simulated with neutral bosonic atoms [14, 15, 16, 17] enable the possibility of tuning the system through quantum phase

transitions and studying real time quantum dynamics. This powerful toolbox for experimentally realizing quantum systems has enhanced the motivation for the study of different quantum models near criticality.

However, there are still some drawbacks in simulating models in optical lattices. The existence of the harmonic confining potential over which the optical lattice is built, puts the atoms (localized in the minima of the optical trap) in a slightly different potential relative to each other and may disturb the uniformity often assumed by theorists.

In this chapter we first review recent experiments that have demonstrated quantum spins realized with cold atoms, and discuss the mapping that allows the identification of the bosons with spins. In Sec. 1.2 we then review the resultant model, the transverse field Ising model. We discuss the quantum phase transition of the model in the presence of an arbitrary field in Sec. 1.3. The study of out of equilibrium dynamics in quantum systems will then be motivated and our approach for studying out of equilibrium dynamics in this model will be briefly explained. This chapter concludes with an outline of the thesis.

1.1 Quantum spins from ultracold atoms

In a recent experiment by Greiner et al. [16], a chain of interacting Ising spins was simulated using a Mott insulator of spinless bosons in a tilted optical lattice. The lattice tilt E is ramped during the experiment until it reaches the on-site interaction energy U, when it induces resonant tunnelling of atoms to their neighbouring site. In the general case of M atoms per site, this produces a "dipole excitation" with a pair of sites with $M-1$ and $M+1$ atoms. The resonance condition is only met when adjacent sites contain equal numbers of atoms, which indicates that neighbouring links can not both have dipoles. The on-site interaction U, and the tunnelling rate t are parameters in the Bose-Hubbard model:

$$H = -t \sum_{<i,j>} {b_i}^\dagger b_j + {b_j}^\dagger b_i + \frac{U}{2} \sum_i \hat{n_i}(\hat{n_i} - 1) - E \sum_i i\hat{n_i}, \tag{1.1}$$

where $< i, j >$ indicates that the sum is restricted to the nearest neighbours, ${b_i}^\dagger$ and b_i are bosonic creation and annihilation operators, $\hat{n_i} = {b_i}^\dagger b_i$ is the number operator on site i, t gives the hopping amplitude to the neighbouring sites, and U is the strength of on-site interactions. When interactions dominate the Hamiltonian, meaning that $t/U \ll 1$, the particles are localized on the lattice sites and

the ground state is a Mott insulator.

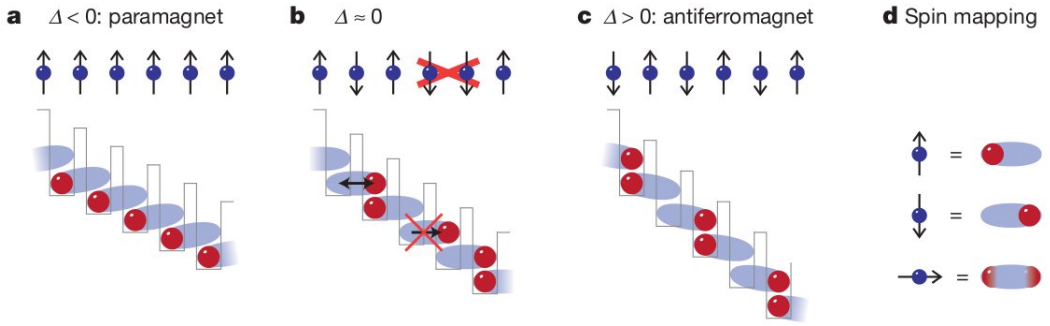

Figure 1.2: Tilted Hubbard model and mapping to spin model [16].

In their experiment, Greiner *et al.* obtained results with $M = 1$ and mapped the Bose-Hubbard model onto a dipole Hamiltonian by defining the dipole creation operator $d_j^\dagger = \frac{b_j b_{j+1}^\dagger}{\sqrt{M(M+1)}}$, and then onto the quantum Ising model (with the interaction parameter J) in the presence of transverse, h_x, and longitudinal, h_z, magnetic fields. The Hamiltonian for this model will be discussed in section 1.3. The mapping was achieved as follows: “spins" were defined through assigning two states to the links between adjacent sites: 0) supporting a dipole excitation and 1) not supporting a dipole excitation, corresponding to “down" and “up" spins respectively. The relation between creation/annihilation of dipoles and the spin operators is as follows:

$$\begin{aligned} S_z^j &= \tfrac{1}{2} - d_j^\dagger d_j, \\ S_x^j &= \tfrac{1}{2}(d_j^\dagger + d_j), \\ S_y^j &= \tfrac{1}{2}(d_j^\dagger - d_j). \end{aligned} \tag{1.2}$$

One can be confident that S_x^j, S_y^j, and S_z^j are the spin operators through checking the commutation relations $[S_\alpha, S_\beta] = i\epsilon_{\alpha\beta\gamma}S_\gamma$. The constraint in the number of the neighbouring dipoles, $d_{j+1}^\dagger d_{j+1} d_j^\dagger d_j = 0$, can be implemented by introducing a positive energy term $J d_{j+1}^\dagger d_{j+1} d_j^\dagger d_j$ to the Hamiltonian, where J is a large coefficient (of order U). This term is the origin of nearest-neighbour spin-spin interaction in their mapping. The initial Mott insulator state maps to the paramagnetic ground state: there is no tunnelling and atoms are localized in individual lattice sites. The transverse field in the equivalent Ising model is responsible for mixing the states, hence arises from tunnelling in the Bose-Hubbard model. The longitudinal field arises from the lattice tilt.

The dimensionless parameters for the Ising model are given by

$$(\tilde{h}_z, \tilde{h}_x) = (1 - \bar{\Delta}, 2^{3/2}\bar{t}), \tag{1.3}$$

where $\bar{t} = t/J$, $\bar{\Delta} = \Delta/J = (E - U)/J$, $J \approx U$ the constraint term, and Δ the energy cost to tunnel.

With increasing tilt strength, the atoms end up occupying the lattice sites as shown in Figure 1.2.c. This corresponds to the opposite alignment of spins of the neighbouring sites in the mapping and addresses the transition to an antiferromagnetic phase. The odd-occupation probability, ρ_{odd}, also confirms (Figure 1.3) the transition from the “paramagnetic" (when all the sites have odd occupation number) to the “antiferromagnetic" phase (when all the sites contain either zero or two atoms).

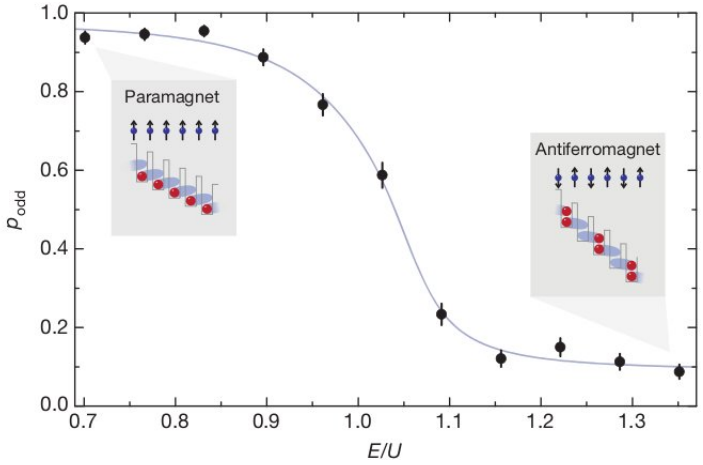

Figure 1.3: “Paramagnetic" to “antiferromagnetic" quantum phase transition in the model of Ref. [16]. The paramagnetic phase in this experiment refers to the phase with no antiferromagnetic order.

This recent study has opened up the possibility of investigating the non-equilibrium dynamics in the transverse field Ising model and has raised a number of questions about the details of the evolution of observables. These questions include how observables generically relax to final stationary values, and how these states depend on the initial states.

1.2 Transverse field Ising model

The Ising model with a transverse field (TFIM) is one of the simplest models that exhibits a quantum phase transition. Simplicity, and the existence of an exact solution for this model (as discussed in

Chapter 2), makes it a good place to study ideas involving quantum phase transitions and out of equilibrium dynamics [18, 19, 20]. Since the early studies of this model in 1960s [9], it has been applied to a variety of problems [8, 21, 22], e.g. atoms in some magnetic materials such as Ho ions in $LiHoF_4$ [23], and Co^{2+} ions in $CoNb_2O_6$ [24] which can acquire two spin states according to their alignment along the crystalline axis and can be represented by two-state Ising spins. Placing these materials in a sufficiently strong external magnetic field h_x transverse to the crystalline axis destroys the order and leaves a magnetically disordered (paramagnetic) phase.

The Hamiltonian takes the form:

$$H = -J \sum_{<ij>} \hat{\sigma}_i^z \hat{\sigma}_j^z - h_x \sum_i \hat{\sigma}_i^x, \tag{1.4}$$

where J is an exchange constant which determines the strength of interactions between nearest-neighbour spins on sites i and j, and h_x is the transverse field. The operators $\hat{\sigma}_i^{z,x}$ are Pauli matrices which act on the different spin states at each site i. A possible basis for spin i is the eigenstates of $\hat{\sigma}_i^z$: $|\uparrow\rangle_i$ and $|\downarrow\rangle_i$, and when $h_x = 0$, the Hamiltonian is diagonal in a basis composed of product states of the form $\prod_i |\sigma_i^z\rangle$. In this case, the ground state is magnetically ordered and the sign of J determines the nature of the ground state. For positive J the ground state is a ferromagnet: the free energy is minimized at $T = 0$ by aligning all the spins in one direction ($+z$ or $-z$). For negative J the preference is the antiparallel alignment of the spins on opposite sublattices, which gives rise to an antiferromagnetic phase.

However, since $\hat{\sigma}_i^x$ is off-diagonal in this basis, increasing h_x will result in mixing the states of the spins. If one continues increasing h_x a phase transition from an ordered state to a disordered state happens at $h_x = h_x^c$ (Figure 1.4). In the limit of $h_x/J \to \infty$, the ground state is a product state of eigenstates of $\hat{\sigma}_i^x$:

$$|\psi_0\rangle = |\rightarrow\rangle_1 \otimes |\rightarrow\rangle_2 \otimes ... \otimes |\rightarrow\rangle_N, \tag{1.5}$$

where $|\rightarrow\rangle_i = \frac{1}{\sqrt{2}}(|\uparrow\rangle + |\downarrow\rangle)_i$. The quantum phase transition can be studied in detail as the model is solvable analytically. The method of solution is to use a Jordan- Wigner transformation [8], which maps the problem of interacting spins to one of non-interacting fermions. The Hamiltonian can then be diagonalized through a Bogoliubov transformation as discussed further in Chapter 2.

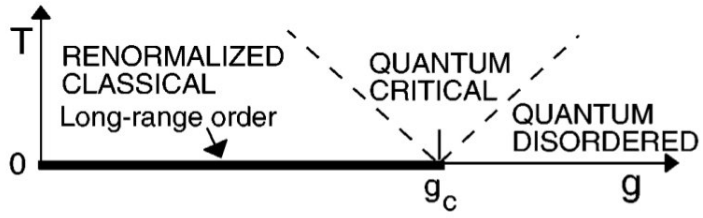

Figure 1.4: Finite temperature phase diagram of model (1.4) [18]. g_c plays the role of h_x^c in our notation..

1.3 Ising model in a mixed longitudinal and transverse field

Adding a longitudinal component h_z to the magnetic field in the Hamiltonian (1.4) allows for a more general magnetic field.

$$H = -J \sum_{<ij>} \hat{\sigma}_i^z \hat{\sigma}_j^z - h_x \sum_i \hat{\sigma}_i^x - h_z \sum_i \hat{\sigma}_i^z. \tag{1.6}$$

This new term changes the phase diagram. For instance, the quantum phase transition in the ferromagnetic model disappears when $h_z \neq 0$ [25]. In antiferromagnetic Ising chains however, the phase transition remains for $h_z \neq 0$ and there is a critical line dividing antiferromagnetic and paramagnetic phases (Figure 1.5).

Although some analytical efforts have been devoted to solving this model in the limit of weak fields (either $h_z/J \ll 1$ or $h_x/J \ll 1$) [25, 26], the exact solution for $h_z = 0$ is not applicable to the more general case. In this case one has to resort to numerical approaches, like the exact diagonalization method (see Chap. 3). However, the exponential growth of the Hilbert space with the size of the system limits the maximum sizes one can achieve in numerical calculations. The largest systems one can treat using the exact diagonalization method depends on the model, for example in a Hubbard chain one may reach 10-20 sites using different variants of the method [27]. This issue has led to the introduction of a series of numerical methods with additional approximations among which the Density Matrix Renormalization Group (DMRG) is known to work very accurately for 1D systems [27].

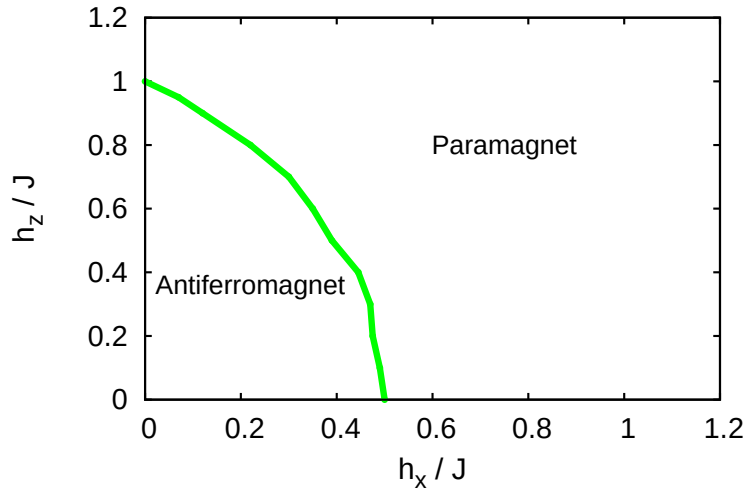

Figure 1.5: The ground state phase diagram of model (1.6) for $J < 0$ obtained from our finite-system DMRG calculations. The critical line separates the antiferromagnetic and paramagnetic phases.

1.4 Out of Equilibrium Quantum Systems

The out of equilibrium dynamics of many-body systems is a long-standing problem, but in quantum systems coupling to the environment and hence dissipation is almost unavoidable. The recent availability of systems that are very weakly coupled to the environment in experiments with cold atoms in optical lattices [15, 16] or trapped ions [28, 29] has provided conditions for studying intrinsic out of equilibrium dynamics of quantum systems for long time scales. Moreover, parameters in cold atom systems can be tuned rapidly in time [15] in a way that is often not possible in condensed matter systems.

A popular protocol for studying out of equilibrium dynamics is performing a quench in one of the system parameters. Quantum quenches in the TFIM have been extensively studied and the dynamics of the order parameter (the magnetization in the ferromagnetic systems, and the staggered magnetization in the antiferromagnetic systems) and some other observables have been investigated: in quenches starting in the paramagnetic phase ($h_x^0 > h_x^c$) to any final transverse field, no long-range order has been found to develop [19]. P. Calabrese *et al.* studied the out of equilibrium dynamics of the one-point and two-point functions of the order parameter in the TFIM analytically [30]. They

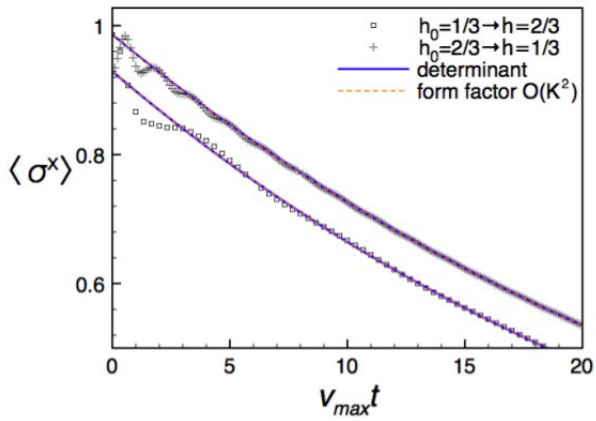

Figure 1.6: Time evolution of $\langle \sigma_x \rangle$ in the model $H = -J \sum_{<ij>} \hat{\sigma}_i^x \hat{\sigma}_j^x - h \sum_i \hat{\sigma}_i^z$ after a quench within the ferromagnetic phase, with $v_{max} = 2Jmin[h, 1]$. Numerical data (obtained from cluster decomposition of the two-point function of the order parameter, $\langle \sigma_{j+l}^z \sigma_j^z \rangle$, at distance $l = 180$) are compared with the asymptotic predictions from both determinants and form factors [30].

showed (Figure 1.6) that for quenches starting from the ferromagnetic phase, the order parameter relaxes to zero exponentially in time (and distance for the two-point function). In quenches starting in the paramagnetic (disordered) phase, the order parameter is zero for all times and the two-point order parameter correlator exhibits oscillatory power-law decay at late times [31]. F. Igloi et al [32] have identified different regimes in the nonequilibrium relaxation of the magnetization profiles of this model. During the time evolution, they observed a decrease in the local magnetization followed by a rapid increase in its value. They interpreted this in terms of quasi particles that are emitted at $t = 0$ and can induce “relaxation" of the observable $(m_l(t))$ when they arrive at the point l or “reconstruction" of the observable by reflecting at the boundaries, passing through the same point, and inducing quantum correlations in time.

The goal of the work here is to study the state after a quantum quench in an antiferromagnetic spin chain in the presence of both transverse and longitudinal magnetic fields. To our knowledge, this problem has not been considered previously. We study the dependence of the evolved observables on the initial state. In Chapter 2 we discuss the analytical solution and the quantum phase transition in the transverse field Ising model. In Chapter 3 we introduce some numerical methods to apply in solving the Ising model in the presence of a mixed field and give an introduction to DMRG. Programming details of implementation of both ground state and time-dependent algorithms are explained and the results are presented in Chapter 4. Chapter 5 is devoted to the conclusions.

Chapter 2

Transverse Field Ising Model

Early studies of the transverse field Ising model (TFIM) date back to the 1960s [8, 9, 21]. The exact solution and the derivation of the phase transition will be discussed in Section 2.1. Theoretical works on the TFIM cover a broad range of research from equilibrium to the out of equilibrium regime [19, 31, 33]. On the experimental side, the model has been realized both in solids [23, 24] and in cold atom systems [16].

The Hamiltonian for an Ising chain of spins in a transverse field is given by

$$H = -J \sum_{i=1}^{N} \sigma_i^z \sigma_{i+1}^z - h_x \sum_{i=1}^{N} \sigma_i^x, \tag{2.1}$$

where J is an exchange constant which sets the microscopic energy scale, and h_x is the transverse field. The quantum degrees of freedom are represented by the Pauli matrices ${\sigma_i}^z$ and ${\sigma_i}^x$ residing on the sites i. The Hamiltonian exhibits a Z_2 symmetry,

$${\sigma_i}^z \rightarrow -{\sigma_i}^z, {\sigma_i}^x \rightarrow {\sigma_i}^x. \tag{2.2}$$

For $h_x/J = 0$ in a ferromagnetic system ($J > 0$), there are two degenerate ground states related by the Z_2 symmetry (Eq. 2.2):

$$\begin{aligned} &|\uparrow_1\rangle \otimes |\uparrow_2\rangle \otimes ... \otimes |\uparrow_N\rangle \text{ , and} \\ &|\downarrow_1\rangle \otimes |\downarrow_2\rangle \otimes ... \otimes |\downarrow_N\rangle, \end{aligned} \tag{2.3}$$

where $|\uparrow_i\rangle$ and $|\downarrow_i\rangle$ are the eigenstates of ${\sigma_i}^z$ corresponding to eigenvalues $+1/2$ and $-1/2$ respectively. The system spontaneously selects one of these ground states. For $h_x/J > 1$ on the

other hand, the ground state is non-degenerate and as the magnetic field is increased, spins acquire larger components along the x direction. This can be explained using the fact that ${\sigma_i}^x$ is off diagonal in the basis of the eigenstates of ${\sigma_i}^z$. Hence turning on a transverse field h_x induces quantum mechanical tunnelling that changes the orientation of spins on a site. Such quantum fluctuations eventually give rise to the transition to a phase where the spins are aligned randomly.

Therefore the model exhibits two phases at zero temperature separating at the critical value of the transverse field, ${h_x}^c = J$: "ferromagnetic" phase when $h_x < {h_x}^c$ and "paramagnetic" phase when $h_x > {h_x}^c$. The order parameter describing this phase transition is the expectation value of the total spin in the z direction, $\langle\psi_0|\sum_i {\sigma_i}^z|\psi_0\rangle$, which becomes zero in the paramagnetic phase.

2.1 The Analytical Solution

The TFIM can be solved exactly using a Jordan-Wigner transformation which maps spin operators onto spinless fermions, represented by fermionic creation and annihilation operators, c_i and ${c_i}^\dagger$, which satisty

$$\begin{aligned} \left\{c_i, c_j^\dagger\right\} &= \delta_{ij}, \\ \{c_i, c_j\} = \left\{c_i^\dagger, c_j^\dagger\right\} &= 0. \end{aligned} \tag{2.4}$$

The transformation is given by

$$\begin{aligned} c_i &= (\textstyle\prod_{j<i} \sigma_j^z)\sigma_i^+, \\ c_i^\dagger &= (\textstyle\prod_{j<i} \sigma_j^z)\sigma_i^-. \end{aligned} \tag{2.5}$$

where $\sigma^\pm = (\sigma^x \pm i\sigma^y)$. The Pauli spin operators, ${\sigma_i}^x$ and ${\sigma_i}^z$, are then transformed as follows [8].

$$\begin{aligned} {\sigma_i}^x &= 1 - 2{c_i}^\dagger c_i, \\ {\sigma_i}^z &= -\textstyle\prod_{j<i}(1 - 2{c_j}^\dagger c_j)({c_i}^\dagger + c_i). \end{aligned} \tag{2.6}$$

After writing the operators in the Hamiltonian (2.1) in terms of c_i and ${c_i}^\dagger$ and simplifying, the Hamiltonian becomes

$$H = -J\sum_{i=1}^{N}[c_i^\dagger c_{i+1} + c_{i+1}^\dagger c_i + c_i^\dagger c_{i+1}^\dagger + c_{i+1}c_i + g(1 - 2c_i^\dagger c_i)], \tag{2.7}$$

where $g = h_x/J$. Note that this form is a special case of the model that supports unpaired Majorana fermions, considered by Kitaev [34] in which the hopping terms have a different coefficient from

the $c_{i+1}c_i$ and $c_i^\dagger c_{i+1}^\dagger$ terms.

Now the Hamiltonian is in a non-interacting form, and it is straightforward to diagonalize. One can start with applying a Fourier transformation to the fermionic operators

$$c_k = \frac{1}{\sqrt{N}} \sum_{j=1}^{N} c_j e^{-ikr_j}, \tag{2.8}$$

and rewriting the Hamiltonian, Eq. (2.6), in momentum space:

$$H = J \sum_k \Big\{ 2[g - \cos(k) {c_k}^\dagger c_k - i \sin(k)[{c_{-k}^\dagger} {c_k}^\dagger + c_{-k} c_k] \Big\}, \tag{2.9}$$

where the lattice spacing is set to unity. The final step in the diagonalization is the application of the Bogoliubov transformation,

$$\gamma_k = u_k c_k - i v_k c_{-k}^\dagger, \tag{2.10}$$

where γ_k is a new fermionic operator and u_k, v_k are real numbers that obey the conditions $u_{-k} = u_k$, $v_{-k} = v_k$, and ${u_k}^2 + {v_k}^2 = 1$. The conditions for u_k and v_k are obtained using the fact that γ_k and ${\gamma_k}^\dagger$, like any fermionic operator, satisfy the anticommutation relations, Eq. (2.4).

Substituting the creation/annihilation operators with γ_k and ${\gamma_k}^\dagger$ in the Hamiltonian (Eq. 2.8), and demanding that the Hamiltonian only contains terms of the form ${\gamma_k}^\dagger \gamma_k$ (so that it would not violate the conservation of the γ fermions), we end up in a constraint on the numbers u_k and v_k. If we set $u_k = \sin(\theta_k)$ and $v_k = \cos(\theta_k)$ (which is valid since it is consistent with the pre-mentioned conditions), then the constraint is given by

$$\tan(\theta_k) = \frac{\sin(k)}{\cos(k) - g}. \tag{2.11}$$

Writing the Hamiltonian in terms of the new fermionic operators (or equivalently θ_k) and using the above constraint, the Hamiltonian can be diagonalized:

$$\begin{aligned} &H = \textstyle\sum_k \epsilon_k ({\gamma_k}^\dagger \gamma_k - \frac{1}{2}), \\ &\epsilon_k = 2J[1 + g^2 - 2g\cos(k)]^{1/2}. \end{aligned} \tag{2.12}$$

Eqs. (2.11) suggest that ϵ_k for all values of k is a finite number as long as $g < 1$. However for $g = 1$, ϵ_0 becomes zero at $k = 0$ indicating zero energy cost for a $k = 0$ excitation. Therefore the

model exhibits a transition from a gapped phase when $g < 1$, to a gapless phase when $g > 1$.

2.2 Mixed Transverse and Longitudinal Field

The transverse field Ising model in spite of being simple and versatile, can not explain several quantum phase transitions, namely, the ones in which an anisotropy of exchange interactions results in a dependence of the magnetic properties on the direction of the applied magnetic field. This has been observed in Cs_2CoCl_4 [35], proposed as a spin $1/2$ one dimensional XY-like antiferromagnet, where the exchange interaction has nonequal values in X,Y, and Z directions, and the magnetic field has both transverse an longitudinal components. It is then important to study the properties of the current quantum mechanical models in the presence of different magnetic fields.

We consider the one dimensional Ising model in mixed transverse and longitudinal fields given by the Hamiltonian

$$H = -J \sum_{<ij>} \hat{\sigma}_i^z \hat{\sigma}_j^z - h_x \sum_i \hat{\sigma}_i^x - h_z \sum_i \hat{\sigma}_i^z. \tag{2.13}$$

There is no exact solution for this model. The Jordan-Wigner transformation applied to the spin operators in the TFIM leaves the transformed Hamiltonian with strings of fermionic creation and annihilation operators that can not be simplified further. The problem has been analytically studied in the limit of weak fields for antiferromagnetic [25] and ferromagnetic [26] systems and the ground state phase transition is found to disappear at $h_z \neq 0$ in the ferromagnetic model. The ground state phase diagram of the antiferromagnetic model was obtained by Ovchinnikov *et al.* [25] both numerically and also through a classical approach (Figure 2.1).

In the classical approximation, Ovchinnikov *et al.* considered spins as three dimensional vectors. The classical ground state configuration is then given by spin vectors lying in the XZ plane with spins on odd and even sites pointing at angles ϕ_1 and $-\phi_2$ respectively, with respect to X axis. The ground state is found by minimizing the classical ground state energy,

$$E/N = -\frac{1}{2}\sin(\phi_1)\sin(\phi_2) - \frac{h_x}{2}[\cos(\phi_1) + \cos(\phi_2)] - \frac{h_z}{2}[\sin(\phi_1) - \sin(\phi_2)], \tag{2.14}$$

as a function of the angles ϕ_1 and ϕ_2. They characterized the antiferromagnetic phase by a nonzero staggered magnetization which vanishes in the paramagnetic phase. Their calculations give the expression for the transition line, dividing the antiferromagnetic and paramagnetic regions in the

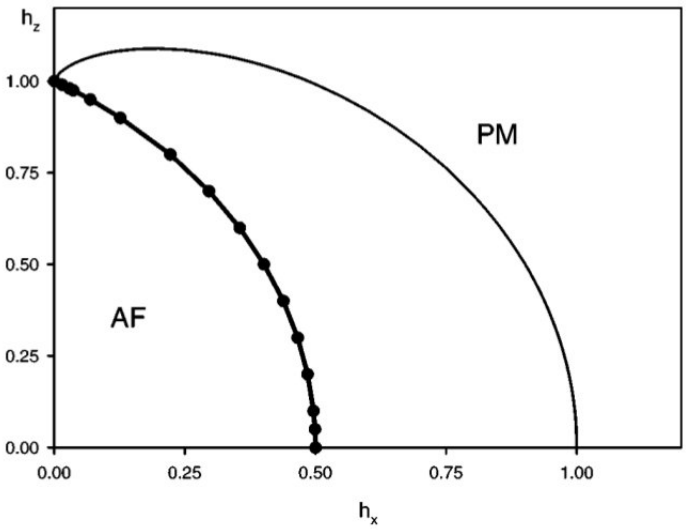

Figure 2.1: The ground state phase diagram of model (1.2) for $J < 0$ obtained in Ref. [25]. The critical line between the antiferromagnetic and paramagnetic phases obtained from the DMRG calculation is shown by thick line and that in the classical approximation by thin line. h_x and h_z are in units of J.

phase diagram, as

$$h_z = \sqrt{1 - {h_x}^{2/3}}(1 + {h_x}^{2/3}), \tag{2.15}$$

shown in Figure 2.1. The classical approach does not provide an accurate description of the phase transition since the phase transition (for any nonzero transverse field) is determined by the quantum fluctuations which in particular, shift the critical point at $h_z = 0$ from $h_x = 1$ to $h_x = \frac{1}{2}$. The addition of the transverse field to the one dimensional classical Ising model, induces quantum fluctuations that can not be taken into account through treating spins as classical vectors. in the Nevertheless, the existence of the two regions with zero and nonzero staggered magnetization in the phase diagram is qualitatively correct and confirmed by numerical calculations using DMRG.

The original motivations for studying this model as discussed at the beginning of the Section, together with the fact that it has not had the same level of attention as the TFIM with $h_z = 0$ and hence is less well known, make this model an interesting case of study for us.

Chapter 3

Numerical Methods

Many condensed matter systems can be reduced to systems of non-interacting particles or quasi particles and hence be described in a single-particle context [36]. However, this mapping may not be applicable to the case of strong correlations within a system with interactions where the full many body problem has to be treated. One possibility to numerically investigate a N-body quantum system is to map it onto a lattice [27] (if it does not naturally live on a lattice). In this case, the state of the system in terms of the site-basis $|\alpha_j\rangle$ is

$$|\psi\rangle = \sum_{\alpha_j} \psi_{\alpha_1\alpha_2...\alpha_N} |\alpha_1\alpha_2...\alpha_N\rangle, \tag{3.1}$$

where $|\alpha_1\alpha_2...\alpha_N\rangle = |\alpha_1\rangle \otimes |\alpha_2\rangle \otimes ... \otimes |\alpha_N\rangle$. Hence the dimension of the basis of the total system is $\prod_{i=1}^{N} s_i$ (s_i being the number of states associated with each site i) which grows exponentially with the size of the system. This is the main restriction in treating the full Hilbert space of a many body quantum system.

A variety of numerical approaches have been introduced to study the low energy properties of such systems. I will discuss some of these methods here, specifically exact diagonalization (ED) and numerical renormalization group (NRG) methods and then introduce the density matrix renormalization group (DMRG) method, which we use in the current work.

3.1 Exact Diagonalization

“Exact Diagonalization" refers to a number of different approaches that produce numerically exact results for a finite system through diagonalizing the system’s Hamiltonian in an appropriate basis. The “appropriate" space can have i) either the same dimension as the Hamiltonian matrix itself, or ii) can be smaller but wisely chosen to represent the correct values of the desired eigenvalues and eigenstates of the Hamiltonian. This is the basic idea behind i) *complete diagonalization* and ii) *iterative diagonalization*.

In complete diagonalization, the entire Hamiltonian matrix has to be stored and diagonalized. Although this is the simplest version of ED and can be used to calculate all desired properties, it is the most memory and time consuming approach. In an Ising spin system with N particles, the dimension of the Hilbert space scales as 2^N and the largest systems one can treat using complete diagonalization, are far smaller than the thermodynamic limit. For example for a Hubbard chain (where the Hilbert space scales faster than 2^N), one may reach less than about 10 sites on a super-computer [27].

To achieve larger system sizes, a series of iterative diagonalization procedures have been introduced. The common idea of such algorithms is to project the matrix on to a subspace (much smaller than the actual Hilbert space) which is chosen so that the extremal eigenstates within the subspace converge to the extremal eigenstates of the system. This reduces the amount of calculations and memory required for diagonalizing the matrix to almost machine precision [37], but is limited to finding the extremal eigenvalues (and the corresponding eigenvectors). One of the main iterative diagonalization approaches used in physics is the *Lanczos* algorithm [38].

Lanczos Algorithm

In 1950 Lanczos proposed his algorithm (which he called the method of minimized iterations) for solving the eigenvalue problem of linear differential and integral operators [38]. In his algorithm the matrix A to be diagonalized is projected onto a smaller subspace in which the projected matrix T is in a tridiagonal form and hence easier to diagonalize. Lanczos suggested a method to construct this subspace so that the extremal eigenvalues of T_M, the leading $M \times M$ part of T, are good approximations to the extremal eigenvalues of A even for $M \ll N$ (where N is the dimension of A).

The algorithm is as follows:

1- Choose an initial vector q_0 to start constructing the aforementioned subspace onto which the Hamiltonian is projected. q_0 must have a nonzero overlap with the ground state of the Hamiltonian to allow for the convergence towards the ground state.
2- Start from $n = 0$ and at the n^{th} step generate the Lanczos basis q_{n+1} through the recursion relation below. Normalize them before going to the next step.

$$|q_{n+1}\rangle = H|q_n\rangle - a_n H|q_n\rangle - b_{n-1}H|q_{n-1}\rangle, \tag{3.2}$$

where $a_n = \langle q_n|H|q_n\rangle$, $b_{n-1} = \|q_{n-1}\|$, $b_0 \equiv 0$, and $|q_{-1}\rangle \equiv 0$.
3- Check if convergence is achieved: $b_n < \varepsilon$: if yes, move to step 4. Otherwise iterate until $n = M$. In the latter case convergence might not be there at the end of the iterations, but eventually it will be achieved through updating the iteration procedure as explained in step 5.
4- Construct the tridiagonal matrix T_M using a_i and b_i found through iterations, and diagonalize it

$$T_M = \begin{pmatrix} a_0 & b_1 & & & \\ b_1 & a_1 & b_2 & \mathbf{0} & \\ & b_2 & a_2 & \ddots & \\ & \mathbf{0} & \ddots & \ddots & b_M \\ & & & b_M & a_M \end{pmatrix}. \tag{3.3}$$

5- Use the eigenvectors of T_M, and Lanczos vectors to find the ground state of the Hamiltonian. Start from step 2 with the ground state as q_0 [39]. Terminate if $b_M < \varepsilon$.

The algorithm returns the ground state wavefunction and energy $E_0 = a_0$.

The number of Lanczos steps needed to converge to the actual ground state of the Hamiltonian is usually much less than the size of the Hilbert space. The implementation of the Lanczos method in this work has allowed us to obtain the ground state eigenvalue and eigenvector of systems with up to $N = 16$ sites (corresponding to a 65536×65536 Hamiltonian matrix), after only about $M \simeq 20 - 50$ Lanczos steps. Going to larger N is restricted by the memory limitations.

This algorithm is much more memory efficient than complete diagonalization in finding the ground state and low-lying excited states since it only stores the 3 vectors q_{n-1}, q_n, and q_{n+1} at each step. Besides, since the Hamiltonian matrices for which Lanczos works the best are sparse, one

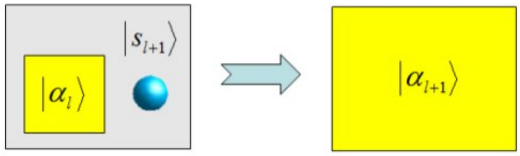

Figure 3.1: Adding a site to the block: a change of basis and a successive truncation.[11].

could store only nonzero elements of the matrix rather than the whole Hamiltonian. This enhances both the speed and memory usage of Lanczos algorithm. However, the largest system size one can treat with any ED method remains limited due to the exponential growth of the Hilbert space with system sizes.

3.2 Numerical Renormalization Group

When the size of the system under consideration gets too large, the computational resources required to diagonalize the matrix are too much and an approximate treatment is required. One such approach is the numerical renormalization group method introduced by Wilson [40] to study the ground state (or low-lying excited states) of large quantum many-body systems. The basic idea in this method is the successive truncation of the Hilbert space by neglecting the “unimportant" degrees of freedom at each renormalization group step. If one is interested in finding the ground state of a system, unimportant degrees of freedom refer to the eigenstates of the system’s Hamiltonian which have the least contribution to the ground state wavefunction. The procedure starts from forming the Hamiltonian H_L for a “block" of the system with length L and gradually adding sites to it. At each step the new Hamiltonian is transformed to a new basis formed by the m eigenvectors of H_L corresponding to the m lowest eigenvalues:

$$\bar{H}_L = O_L^\dagger H_L O_L. \tag{3.4}$$

Here O_L is the transformation matrix whose columns are the m lowest eigenvectors of H_L. Next, a single site, with an associated D dimensional Hilbert space, is added to the current block to form the new system’s Hamiltonian H_{L+1} (Figure 3.1). The whole procedure is restarted with H_{L+1}. In this method the dimension of Hilbert space of the Hamiltonian to be diagonalized, $D \times m$, is maintained constant which allows the method to be used to treat very large system sizes.

However, this procedure does not work well for a number of lattice models including the one-dimensional Heisenberg and Hubbard models and loses accuracy after a few iterations [27]. A precise analysis of the origin of this inaccuracy is hard for many-body problems but it was identified by Wilson using a toy model of a single particle on a tight-binding chain [41]. In this model due to the simpler non-interacting nature of the problem, one can modify the NRG method to carry out a more efficient diagonalization: since the dimension of the Hilbert space here grows much slower than in an interacting system, instead of adding single sites at a time, two equal-sized blocks can be put together at each step. In one iteration, when the length of the system grows from L to $2L$, a linear combination of the lowest few eigenstates of the L-site system is used to approximate the wavefunction of the larger system. For the case of fixed boundary conditions the eigenfunctions have the form

$$\psi_n{}^L(l) \propto \sin\left(\frac{n\pi l}{L+1}\right), \tag{3.5}$$

where $n = 1, ..., L$. Therefore, as can be seen in Figure 3.2, the combination of two $\psi_n{}^L(l)$ leads to a “kink" at the boundary between blocks which clearly makes it a bad approximation to the ground state of the larger system.

This is a simple example to show that treating the boundaries of the subsystem blocks in NRG is an important issue. Several methods have been suggested to overcome this problem. Applying a general set of boundary conditions to the subsystem blocks, and the “superblock method" are found to be some of the most effective solutions [42].

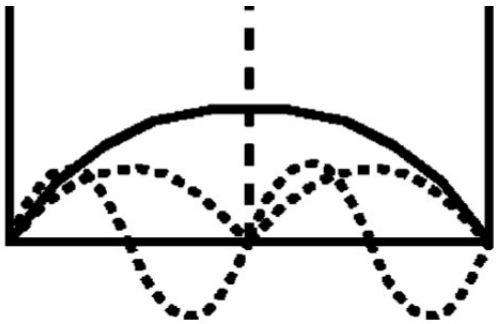

Figure 3.2: The lowest-lying eigenstates of two initial blocks (dashed line) and a double-sized block (solid line) for the problem of a single particle in a box [41].

3.2.1 Superblock Method

The idea of the superblock method is that the individual blocks that are put together at each step constitute part of a larger system: the “superblock". In this method, after putting two blocks of length L together, a new basis will be formed for the Hamiltonian H_{2L}. In order to do this, a superblock is formed by putting together $p > 2$ blocks. After diagonalizing the Hamiltonian of the superblock H^p_{2L}, the transformation matrix O_{2L} is constructed to project the m lowest-lying eigenstates of the superblock onto the coordinates of the first two blocks. The whole procedure is then restarted with the two blocks in the transformed basis.

The idea of embedding the blocks in a larger superblock allows for considering the fluctuations in the surrounding blocks and is effectively a substitute for applying general boundary conditions [27]. In spite of successes in describing noninteracting systems using the superblock method, generalizing it to the case of interacting systems is not trivial. One state of the superblock can project onto more than one state of the subsystem blocks since the total Hilbert space is not a direct sum of those of the subsystems in the interacting problems. The “density matrix renormalization group" method optimally carries out this projection.

3.3 Density Matrix Renormalization Group

The density matrix renormalization group (DMRG) was introduced by Steven White in 1992 [43] as an extension of Wilson’s NRG. Since its introduction, it has found applications far from its origin in condensed matter, to fields such as quantum chemistry of small molecules [44], physics of small superconducting grains [45], and equilibrium and out of equilibrium problems in quantum statistical mechanics (which will be discussed in Section 3.3.3).

The main feature of DMRG is its ability to treat large systems at high precision very close to zero temperature. The remarkable accuracy of DMRG has been illustrated in several models, for example the spin-1 Heisenberg chain, where a precision of 10^{-10} for the ground-state energy of a system with hundreds of sites was obtained using DMRG [46]. DMRG is most powerful for one-dimensional systems [41]. Nevertheless, interesting improvements to treat systems in higher dimensions have also been made [47, 48].

To understand why large systems and high accuracy are accessible by DMRG, we have to go back to the problem mentioned earlier: What is the optimal way to carry out the projection of the

wave function of a system onto its subsystems?

3.3.1 Density Matrix Projection

The density matrix is the most general description of a quantum mechanical system. For a system U in a pure state ψ, the state of the subsystem S is given through the reduced density matrix

$$\rho_S = Tr_E|\psi\rangle\langle\psi|, \tag{3.6}$$

where the trace is over the states of the other subsystem E. U, S, and E are traditionally chosen to refer to the *universe*, *system*, and *environment* blocks. The expectation value of an observable $\hat{A}$ acting on the system block can be written in the density matrix eigenbasis $|w_i\rangle$ ($\rho_S|w_i\rangle = w_i|w_i\rangle$) as

$$\langle\hat{A_S}\rangle = \sum_i w_i\langle w_i|\hat{A}|w_i\rangle. \tag{3.7}$$

Now if the contribution of some eigenvectors of ρ_S to $\langle\hat{A_S}\rangle$ is negligible (meaning that they correspond to negligible eigenvalues) one would make a small error by neglecting them in the above equation and projecting the state onto the most dominant eigenvectors of the reduced density matrix. This in fact forms the kernel of the DMRG method: systematic truncation of the Hilbert space by keeping only the most probable states describing accurately the target state (here, the ground state).

The maximum number of states m that need to be kept in a DMRG algorithm for obtaining a desirable accuracy varies in different models depending on how fast the density matrix eigenvalues decay. Higher precision (when m is large) is traded for treating larger systems (when m is small). A comparison of the resultant accuracy for different values of m will be presented shortly after the introduction of DMRG algorithms and other control parameters.

3.3.2 DMRG algorithms

In Section 3.3.1 we introduced the idea of using the density matrix to truncate the Hilbert space within the superblock method. In the density matrix renormalization group (DMRG) it is important to specify how to grow the superblock and add degrees of freedom. Two possible suggestions are either i) growing both blocks to reach larger systems at each step or ii) growing one block while shrinking the other, to investigate a system with a finite length. These two different approaches construct the two versions of DMRG algorithms: infinite-system and finite-system.

Infinite System Algorithm

In the infinite system algorithm both the system and environment block grow by a single site at each step. The superblock is then enlarged two sites at a time until the desired length is achieved. For an infinite system the criterion for stopping iterations is the convergence of the energy and observables to some final values.

This algorithm aims to find the ground state energy and wave function of the system and proceeds as follows:

1- Consider an initial system and environment block, each with length l, where l is small enough to allow for exact diagonalization.
2- Form the new system block by adding a single site to it. Write the Hamiltonian for the current block H_S^{l+1} using H_S^l and the added interactions between the single site and the old block. Form the new environment block of length $l' = l + 1$ in a similar way.
3- Construct the superblock Hamiltonian. Diagonalize it using a sparse-matrix-diagonalization method like Lanczos to find the ground state eigenvalue and eigenvector ψ.
4- Find the reduced density matrix for the system block by tracing over the states of the environment block:

$$\rho_{ii'} = \sum_j \psi^*_{ij}\psi_{i'j}, \tag{3.8}$$

where $\psi_{ij} = \langle i|\langle j|\psi\rangle$, and $|i\rangle$ and $|j\rangle$ are the basis of the system and environment blocks respectively. Diagonalize it and sort its eigenvalues in descending order. Do the same with the environment block.
5- If the dimension of Hilbert space of the system block exceeds the number of states to keep, truncate it to a new truncated basis by acting with a transformation matrix T_S on the Hamiltonian and all the observables: ${H'_S}^{l+1} = {T_S}^\dagger H_S^{l+1} T_S$. T_S is a rectangular matrix whose columns are the m eigenvectors of the reduced density matrix with the largest eigenvalues. Truncate the environment block similarly.
6- Start from step 2, with the $l + 1$-site system (environment) block as the old system (environment) block.

Measuring the desired observables can also be included in the above procedure. The details of mea-

surement will be discussed in the following section. In the infinite system algorithm, one could choose the environment block to be a reflection of the system block to reduce the number of computational steps. This is valid only for reflection symmetric systems. For systems that lack this symmetry two subsystem blocks need to be treated separately.

However, the infinite system algorithm does not produce accurate results in some systems [41, 49]. This inaccuracy originates in the varying size of the system that is being diagonalized at each step. For an infinite system, running DMRG with small blocks in the early steps can result in a poor convergence or it may trap the system in a metastable state corresponding to a local minimum in the energy of systems with small sizes [41]. This motivates the introduction of an algorithm that treats the same size superblock at each step to avoid this problem.

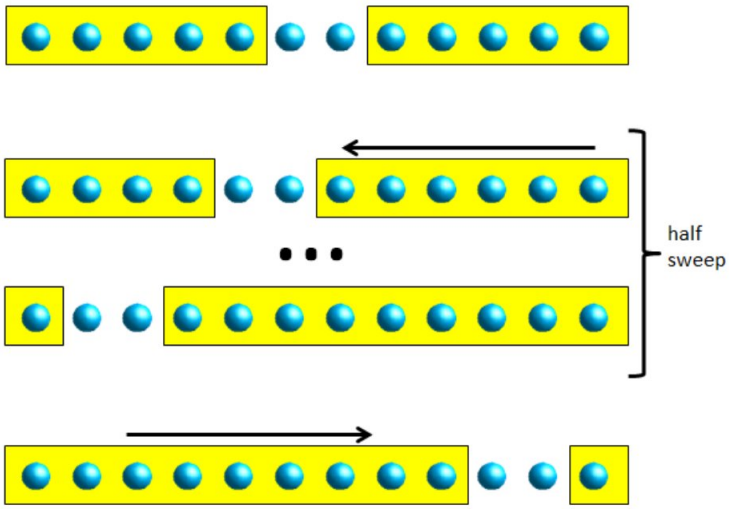

Figure 3.3: Schematic illustration of the finite-size DMRG algorithm. During the sweeping iterations, one block grows, and the other one shrinks. The shrinking block is retrieved from the blocks obtained in the previous sweep in the opposite direction, which are stored in memory or disk [11].

Finite System Algorithm

In the finite system algorithm the size of the superblock, L, is kept constant. At each step the system block grows by a single site at the expense of reducing the environment's length by one. This procedure continues until the environment block has been shrunk to a single site. Then the growth direction is reversed: the environment block expands and the system block starts to shrink in

a similar way. A "sweep" is completed at this point (Figure 3.3). At each step the Hamiltonian and operators acting on the shrunk block are restored from the previous finite system sweep (or from the infinite system algorithm for the first sweep). Truncation is performed only on the expanding block. After a few sweeps the energy and wave functions of the L-site superblock will be obtained.

A finite system algorithm proceeds as follows:

1- Run the infinite system algorithm until the superblock reaches the desired length L. Store the Hamiltonian and the required operators of the blocks at each step.

2- Carry out steps 2-6 of the infinite algorithm until $l = L - 3$. At this value of l, use the stored value for $H_E^{l'}$ ($l' = L - l - 2$) instead of using H_E^l for building the current environment block's Hamiltonian. Store the current Hamiltonian for both blocks.

3- Similarly to step 2, expand and shrink the environment and system block respectively until $l = 1$.

4- Repeat steps 2-3 until convergence is achieved.

Error in the finite system algorithm can be decreased to almost the truncation error, i.e. the error in neglecting some of the eigenvectors of the reduced density matrix [41]. The accuracy of this algorithm can be controlled by varying the maximum number of states to keep and the number of sweeps (Figure 3.4).

While the accuracy of the finite system algorithm is considerably higher than the infinite system algorithm, its running time is greater. The computational cost of the finite-system DMRG scales as $O(Nm^3)$ [50] and in general, every sweep takes about four times the CPU time of the starting infinite-system DMRG calculation. However one can decrease the running time for a finite system DMRG program significantly without adversely affecting the accuracy. This can be achieved due to the fact that the dependence of the accuracy on the number of states kept in the truncation procedure is weak when there are a small number of sweeps [27]. Therefore one can start from a small number of states and gradually increase it through sweeps.

Despite reliable results produced by finite system DMRG, there is still always a possibility of being trapped in a local minimum state. To minimize this risk one needs to study the stability of the final results over the course of successive iterations and perform a sufficient number of sweeps to achieve convergence to the true minimum energy of the system.

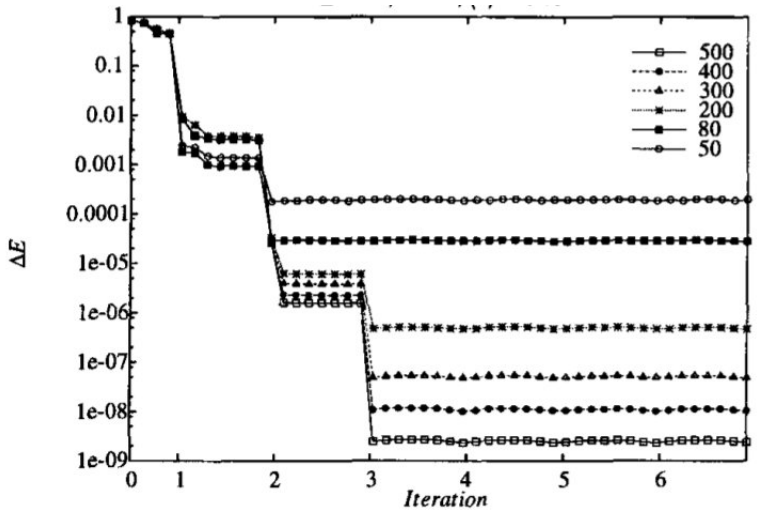

Figure 3.4: Difference between the ground state energy obtained from the finite system DMRG with different number of sweeps and number of states kept m, and the exact energy calculated using Bethe Ansatz for a 32-site Hubbard model. [27].

Moreover, the powerful DMRG technique for one dimensional systems, does not work as well for two dimensional problems. This arises from the relatively large boundary and hence large number of connections between the system and environment blocks which leads to attaining a given accuracy with keeping many more states in the density matrix truncation [27].

3.3.3 Programming Details

Application of the DMRG method in different problems requires a deep understanding of the constructing elements of a DMRG algorithm. Other than the several steps listed earlier in the DMRG algorithms, there are some other elements that are not part of the main body, but necessary to do measurements using DMRG or to increase its efficiency.

3.3.3.1 Measurements

The wave function obtained by DMRG can be used to calculate the expectation value of operators. In a transverse field Ising chain, as given in Eq. (1.1), some of the interesting observables to measure are the expectation value of the magnetization $\langle\psi_0|\sum_{i=1}^{N} S_i^z|\psi_0\rangle$, or two-point correlation functions $\langle\psi_0|S_i^z S_j^z|\psi_0\rangle$. The operators of interest have to be presented in the current basis, hence they have to be transformed at each step, similarly to the transformation of the left/right block Hamiltonian.

The single-site expectation value of an operator O acting on site l (assume it belongs to the left block) is given by

$$\langle\psi|O_l|\psi\rangle = \sum_{i,i',j} \psi^*_{ij}[O_l]_{ii'}\psi_{i'j}, \tag{3.9}$$

where $|i\rangle$ and $|i'\rangle$ are in the left block basis and $\{|j\rangle\}$ is the right block basis. The matrix representation $[O_l]_{ij}$ is first constructed when site l is added to the system, and then is transformed at each step so that it is presented in the basis $\{|i\rangle\}$.

For expectation values of operators on multiple sites, their matrix representation and transformation depends on whether they operate on the same block or on different blocks. If O_l and O_m act on the single sites in the left and right block respectively,

$$\langle\psi|O_lO_m|\psi\rangle = \sum_{i,i',j,j'} \psi^*_{ij}[O_l]_{ii'}[O_m]_{jj'}\psi_{i'j'}. \tag{3.10}$$

However, if sites l and m belong to the same block,

$$\langle\psi|O_lO_m|\psi\rangle = \sum_{i,i',j} \psi^*_{ij}[O_lO_m]_{ii'}\psi_{i'j}. \tag{3.11}$$

In this case instead of calculating the individual single-site operators $[O_l]_{ii'}$ and $[O_m]_{jj'}$, one has to calculate the composite product operator $[O_lO_m]_{ii'}$ at the appropriate step and transform it successively during the DMRG sweeps.

3.3.3.2 Wave Function Transformations

The most time consuming part of the DMRG algorithm is the exact diagonalization of the superblock Hamiltonian at each step. Hence improving this part of the algorithm can speed up the total procedure significantly. One possibility is using an appropriate initial guess as the seed for the exact diagonalization method. If the Lanczos procedure starts with a vector that is a good approximation to the desired wave function, many fewer iterations are required before convergence is achieved. The wave function in the previous DMRG step seems to be a good approximation to the wave function at the current step, but is presented in a different basis. Therefore an algorithm to transform the wave function from one step to the next one is needed.

At step l, when the basis of the left block (containing sites $1, ..., l$) is $|\alpha_l\rangle$, and the basis of the right block (containing sites $l+3, ..., L$) is $|\beta_{l+3}\rangle$, the wave function is calculated in the superblock

basis,

$$|\alpha_l s_{l+1} s_{l+2} \beta_{l+3}\rangle \equiv |\alpha_l\rangle \otimes |s_{l+1}\rangle \otimes |s_{l+2}\rangle \otimes |\beta_{l+3}\rangle, \tag{3.12}$$

where $|s_{l+1}\rangle$ and $|s_{l+2}\rangle$ are the bases of the single sites $l+1$ and $l+2$.

At the next step (if we assume the sweep is left to right), the wave function will be in the basis

$$|\alpha_{l+1} s_{l+2} s_{l+3} \beta_{l+4}\rangle, \tag{3.13}$$

where $|\alpha_{l+1}\rangle$ and $|\beta_{l+4}\rangle$ are the effective density matrix bases obtained at the end of the previous step and can be written in terms of the original product bases via the following transformations [51]:

$$\begin{aligned} |\alpha_{l+1}\rangle &= \textstyle\sum_{s_{l+1},\alpha_l} (U_L{}^{\dagger})_{\alpha_{l+1},\alpha_l s_{l+1}} |\alpha_l\rangle \otimes |s_{l+1}\rangle, \\ |\beta_{l+3}\rangle &= \textstyle\sum_{s_{l+3},\beta_{l+4}} (U_R)_{s_{l+3}\beta_{l+4},\beta_{l+3}} |s_{l+3}\rangle \otimes |\beta_{l+4}\rangle. \end{aligned} \tag{3.14}$$

U_L and U_R contain the density matrix eigenvectors and are simple rearrangements of the matrix elements of the transformation matrices T_S for the left and right blocks used in transforming the Hamiltonian of the blocks to the new basis [52].

By assuming $\sum_{\alpha_{l+1}} |\alpha_{l+1}\rangle\langle\alpha_{l+1}| = 1$ (which is an approximation since the Hilbert space is truncated), the wave function in the new basis becomes

$$|\psi\rangle = \sum_{\alpha_l s_{l+1} \beta_{l+3}} (U_L{}^{\dagger})_{\alpha_{l+1},\alpha_l s_{l+1}} (U_R)_{s_{l+3}\beta_{l+4},\beta_{l+3}} \langle \alpha_l s_{l+1} s_{l+2} \beta_{l+3} | \psi \rangle |\alpha_{l+1} s_{l+2} s_{l+3} \beta_{l+4}\rangle. \tag{3.15}$$

For the right to left half-sweeps a similar transformation is used.

Adding the above procedure (known as the “wave function prediction" introduced by White [53]) to the main DMRG algorithm involves storing the transformation matrices at every step which makes it a little expensive in the memory usage. However, it is still relatively inexpensive in CPU time and memory compared to other steps of the DMRG procedure, and of course reduces the calculations in the iterative digonalization at each single DMRG step.

Although the idea of using the old wave function at the current step was introduced as an optional step in the DMRG algorithm, it is an inseparable part of the time-dependent DMRG algorithm as will be discussed in the next section.

3.3.4 Time Dependent DMRG

The study of nonequilibrium dynamics in quantum systems is motivated by a variety of physical phenomena in the fields of spintronics, low dimensional correlated systems, quantum computing [54], and recently cold atom experiments. Therefore the accurate calculation of time dependent quantum observables in such systems has attracted considerable attention.

Some of the existing numerical methods for the investigation of strongly correlated quantum systems are quantum Monte-Carlo (QMC) [55], exact diagonalization (ED) and DMRG. There have been some attempts to calculate time-dependent quantities in quantum systems using these methods. QMC has been extended to the time dependent regime [56, 57], however these calculations are difficult to control [58]. Implementation of ED to account for time evolution on the other hand, can easily allow one to calculate many desired quantities, but is limited to small systems as discussed earlier.

Using DMRG to calculate time dependent observables is probably the best method for sufficiently large one dimensional systems. The main issue in the study of time evolution with DMRG is that the truncated subspace of the system's Hilbert space that represents the initial state of the system might not be appropriate to properly determine the state at later times. This reflects the fact that there might be regions of the Hilbert space that are discarded in DMRG which the wave function might explore in its subsequent evolution in time.

This problem was first pointed out by Luo *et al.* [59] in a comment on a "time-dependent DMRG" (TdDMRG) method introduced by Cazalilla and Marston [60]. In the TdDMRG method the time-dependent Schrodinger equation was numerically integrated in time in a fixed reduced Hilbert space after applying a standard DMRG calculation. Luo *et al.* argued that by working within a static reduced Hilbert space (in which the initial state is represented), the long time behaviour becomes poor since the time evolution of the initial state evokes excited states in a nonequilibrium system which might not be represented in the initial reduced Hilbert space. Their suggestion for solving this problem was to include states at all time steps in the density matrix. They showed that targeting the entire range of time enlarges the initial reduced Hilbert space and allows for retaining the information on the relevant excited states. This method still uses a static Hilbert space but tries to use a basis that includes all the states that the system explores in the course of time evolution (Figure 3.5).

However, this method has the disadvantage of targeting states at all time steps which requires a

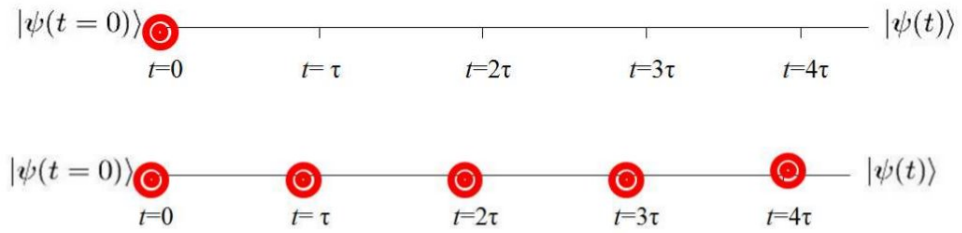

Figure 3.5: The top figure illustrates the original idea of TdDMRG: The initial state is calculated and evolved in time by numerically integrating the Schrodinger equation. The figure at the bottom shows Luo *et al.*'s idea of targeting the states at every time-step, keeping track of the entire time-evolution of the wave function. [11].

large number of density matrix eigenstates to be kept and slows down the calculations.

A more efficient time-dependent DMRG is the so called adaptive tDMRG [61, 62]. In this method instead of directly integrating the Schrodinger equation in a fixed space, the states kept in the reduced basis are adjusted at each step to represent the state of the system at the next step, hence the basis changes dynamically as we proceed in time.

Suzuki-Trotter Approach

The implementation of the Suzuki-Trotter (S-T) decomposition of the time evolution operator in an adaptive tDMRG algorithm was first formulated by White and Feiguin [62]. In this approach, due to the change of the effective Hilbert space at each time step, the total evolution time is split into N small intervals and the time evolution operator is successively performed on the state of the system at each time step:

$$u(t) = e^{\frac{-iHt}{\hbar}} = (e^{\frac{-iH\Delta t}{\hbar}})^N \tag{3.16}$$

To obtain the time evolved state $|\psi_{(t+\Delta t)}\rangle = e^{\frac{-iH\Delta t}{\hbar}}|\psi_{(t)}\rangle$ S-T decomposition of the matrix exponential $e^{\frac{-iH\Delta t}{\hbar}}$ is used. To first order one has

$$e^{-\frac{i}{\hbar}H\Delta t} \approx e^{-\frac{i}{\hbar}H_A\Delta t}e^{-\frac{i}{\hbar}H_B\Delta t} + O(\Delta t^2), \tag{3.17}$$

where H_A contains the terms of the Hamiltonian for the even links, and H_B for the odd links. Since the individual link-terms $e^{-\frac{i}{\hbar}H_j\Delta t}$ (coupling sites j and $j+1$) within H_A or H_B commute, one can write

$$e^{-\frac{i}{\hbar}H_A\Delta t} = e^{-\frac{i}{\hbar}H_1\Delta t}e^{-\frac{i}{\hbar}H_3\Delta t}\cdots. \tag{3.18}$$

This allows application of the bond time evolution operator $e^{-\frac{i}{\hbar}H_j\Delta t}$ on individual even links during a DMRG half-sweep, and on individual odd links in the next half sweep. The bond evolution operators have a very simple matrix representation which can be found easily by considering the single site terms and the nearest-neighbour interactions in the Hamiltonian.

The error in this method is the Trotter error which can be controlled by using higher order decompositions and hence doing more DMRG sweeps. For example, the second order Suzuki-Trotter decomposition is

$$e^{-\frac{i}{\hbar}H\Delta t} \approx e^{-\frac{i}{\hbar}H_A\Delta t/2}e^{-\frac{i}{\hbar}H_B\Delta t}e^{-\frac{i}{\hbar}H_A\Delta t/2} + O(\Delta t^3). \tag{3.19}$$

The main advantages of the S-T method are: the simple form of the local evolution operators, the small amount of calculations in multiplying small matrices by the wave function, and the control over decreasing the error by simply doing some more sweeps along the system.

Time-Step Targeting

In spite of the efficiency and accuracy of the S-T method, it is limited to Hamiltonians with only nearest neighbour interactions. To study a problem with longer range interactions one alternative is to modify the original proposal of Luo *et al.* [59] to adapt the basis in a similar fashion as the S-T approach, but possibly without keeping track of the entire history of the state. "Time-step targeting" (TST) was the name originally used to refer to this method [51]. In this approach, at each time step a basis is produced, targeting the states needed to represent one time step. Once the adaptation to the new basis is complete, the time step is taken and the algorithm proceeds to the next time step. Hence, similarly to Ref. [59] a number of wave functions at a sequence of times is used to form the density matrix, but this happens at every single time step (Figure 3.6).

What intermediate states do we use in the density matrix? In the original proposal, the states at times t, $t+\tau/3$, $t+2\tau/3$, $t+\tau$ appear in the density matrix at time t with the respective weights of $1/3$, $1/6$, $1/6$, $1/3$. The standard fourth-order Runge-Kutta (R-K) algorithm is applied to construct

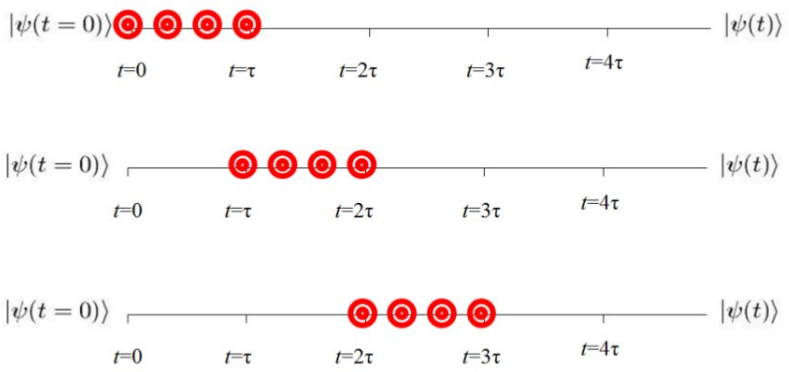

Figure 3.6: Time-step targeting idea: at every time step, target four intermediate states to optimize the basis for the time evolution. [11].

the intermediate states by defining a set of four vectors

$$\begin{aligned} |k_1\rangle &= \tau \tilde{H}_{(t)}|\psi_{(t)}\rangle, \\ |k_2\rangle &= \tau \tilde{H}_{(t+\tau/2)}[|\psi_{(t)}\rangle + 1/2|k_1\rangle, \\ |k_3\rangle &= \tau \tilde{H}_{(t+\tau/2)}[|\psi_{(t)}\rangle + 1/2|k_2\rangle, \\ |k_4\rangle &= \tau \tilde{H}_{(t+\tau)}[|\psi_{(t)}\rangle + |k_3\rangle, \end{aligned} \tag{3.20}$$

where $\tilde{H}_{(t)} = H_{(t)} - E_0$. The states are then obtained as follows [51]

$$\begin{aligned} |\psi_{(t+\tau/3)}\rangle &\approx \tfrac{1}{162}[31|k_1\rangle + 14|k_2\rangle + 14|k_3\rangle - 5|k_4\rangle] + O(\tau^4), \\ |\psi_{(t+2\tau/3)}\rangle &\approx \tfrac{1}{81}[16|k_1\rangle + 20|k_2\rangle + 20|k_3\rangle - 2|k_4\rangle] + O(\tau^4), \\ |\psi_{(t+\tau)}\rangle &\approx \tfrac{1}{6}[|k_1\rangle + 2|k_2\rangle + 2|k_3\rangle + |k_4\rangle] + O(\tau^5). \end{aligned} \tag{3.21}$$

Comparing TST and Luo *et al.*'s method, TST requires less density matrix eigenstates to be kept since it targets a narrower range of time. This leads to less computational cost and faster performance time of TST. However, TST is not as efficient as the S-T method since it targets more than one state at a time and needs to keep a larger number of states to achieve the same accuracy as S-T [51]. This is of course the price TST pays in the exchange for the ability to treat longer-range interactions which is not achievable by S-T (for an extensive analysis and comparison of errors in these two methods see the original paper [51].)

The algorithm for implementing TST method proceeds as follows:

1 Run ground-state DMRG to calculate the initial state.

2 Introduce a perturbation to the problem: such as a change in the Hamiltonian or the state.

3 Turn off the Lanczos: the state of the system is no longer obtained through ED, it is instead transformed to the adapted basis from step to step.

4 Start the sweeping process:

   1 Find the intermediate states through the R-K procedure, use them to form the density matrix $\rho = \sum_t w_t |\psi_t\rangle\langle\psi_t|$ with the corresponding weights.

   2 Increase the block size by adding a site, apply the same density matrix truncation as in the ground-state algorithm.

   3 Rotate all the operators to the new basis.

   4 Rotate the wave function to the new basis by using the wave-function prediction explained in section 3.3.2.2.

5 Advance in time after the completion of one (or more, for producing a better basis for the time step) half-sweeps. Start from step 4 with the new wave function until the desired number of time steps has been taken.

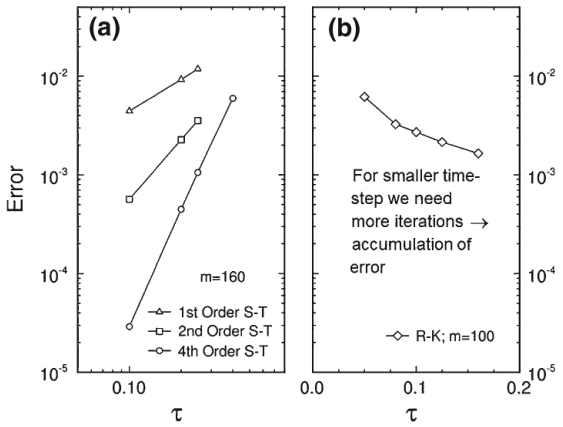

Figure 3.7: Error at t=8 (in units of the Heisenberg exchange J) for the Haldane chain for different time steps τ. a) Suzuki-Trotter method; b) TST method using Runge-Kutta. [11].

The two fundamental sources of error in tDMRG are i) The truncation error, and ii) the error introduced in taking the integration (R-K) or the time evolution using S-T method. The truncation error, the error we make by throwing away some eigenstates of the density matrix, can be controlled by keeping more states, and the error in the integration can be controlled by decreasing the time step τ. In TST the error is almost dominated by the truncation error [11] and hence it accumulates with the number of steps. Therefore although one would first expect to obtain smaller error with smaller time steps (as in the S-T method), the greater the number of iterations needed to reach a desired time with smaller τ, the larger accumulation of errors (Figure 3.7, 3.8).

Moreover, the truncation error typically grows in time for a sudden quench. This reflects the fact that upon such a perturbation, the system is no longer in the ground state but in a superposition of some excited states. If insufficient density matrix states are kept, the weight of such "unwanted" states increases in time. Therefore, increasing the number of states m with time, is a solution for maintaining the error small for larger times. The rate of changing m for an efficient simulation in a sudden global quench is $m(t) \sim \exp(t)$ [11]. Consequently the required number of states may quickly grow to a point when it becomes unmanageable by the computer. At this point, continuing the time evolution with a fixed m may lead to unreliable results. Attempts to extend the use of tDMRG to longer time scales constitutes a major part of recent studies in the field [63, 64].

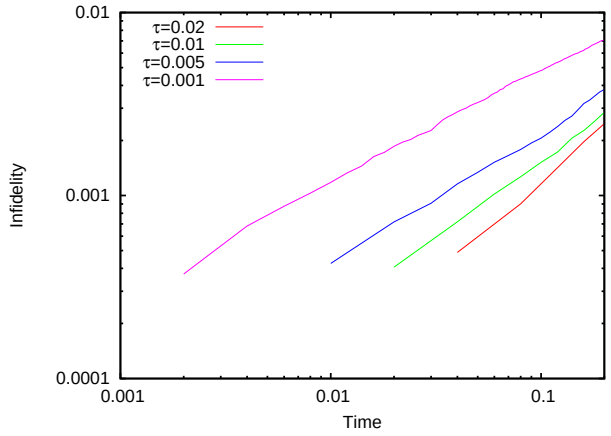

Figure 3.8: Infidelity, $1 - |\langle\psi_t|\psi_0\rangle|$, for the transverse field Ising chain of 20 sites, for different time steps τ, obtained from our finite-system DMRG simulations. In this simulation 8 sweeps are completed before the beginning of the time evolution, 1024 states are kept, and $h_x/J = 0.8$. Time measured in units of $\hbar/J$.

Chapter 4

Results

In this Chapter we present the results obtained from our exact diagonalization (ED) and DMRG simulations of the transverse field, and mixed fields Ising model (Eqs. 2.1 and 2.12). We first test the results of our exact diagonalization and DMRG algorithms through a study of the order parameter in the course of the quantum phase transition discussed in Chapter 2. The order parameters we consider are the magnetization

$$M^z = \frac{1}{N}\langle\psi_0|\sum_{i=1}^{N} S_i^z|\psi_0\rangle, \tag{4.1}$$

in ferromagnetic systems and the staggered magnetization

$$N^z = \frac{1}{N}\langle\psi_0|\sum_{i=1}^{N} (-1)^i S_i^z|\psi_0\rangle, \tag{4.2}$$

in antiferromagnetic systems, which we calculate using the ground state wave function ψ_0. We then present the results of our tDMRG simulation in which we have used ED and DMRG. We compare our results for the TFIM with the literature and investigate the behaviour of the order parameter in different quenches in the antiferromagnetic Ising chain given by Eq. 2.12.

4.1 Exact Diagonalization

In this section we present the results for numerically solving the TFIM with the Lanczos method. The ground state eigenstate and energy are obtained for different values of the transverse field h_x/J. Using the ground state wave function of a ferromagnetic system with N spins, the magnetizations

in the z direction, M^z, and the x direction, M^x are obtained. M^z and M^x in different systems are shown as a function of the field h_x/J in Figures 4.1 and 4.2. As discussed earlier in Chapter 2 the

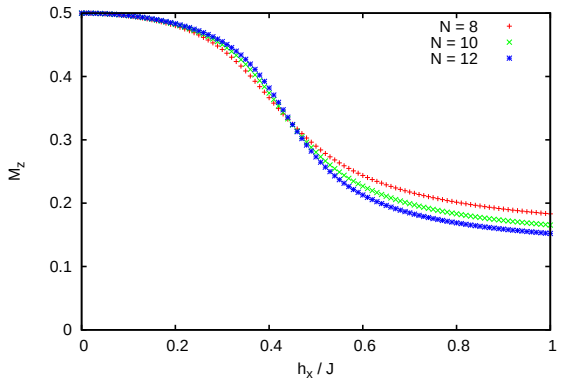

Figure 4.1: M^z for the ferromagnetic transverse field Ising model as a function of h_x/J for different values of system sizes N calculated by our Lanczos simulation.

ground state of a transverse field Ising chain exhibits an “ordered" and a “disordered" phase. The two phases in ferromagnetic systems correspond to $M^z \neq 0$ and $M^z = 0$ respectively. In fact for $h_x = 0$ all the spins are aligned along the z axis and M^z attains its maximum value while $M^x = 0$. By increasing the field, M^x grows and above the critical value, $h_x^c/J = 1/2$, M^z vanishes in the thermodynamic limit and M^x continues growing so that as $h_x/J \to \infty$ it saturates to its maximum value of $\frac{1}{2}$. Note that the difference in the value of the critical field between our results and $g^c = 1$ obtained in Chap. 2 comes from treating the spin operators, $S_i^\alpha = \frac{\hbar}{2}\sigma_i^\alpha$, rather than the Pauli matrices σ_i^α.

For finite system sizes N, the magnetization vanishes as

$$\left\langle \frac{1}{N}\sqrt{\left|\sum_i S_i^z\right|^2} \right\rangle \approx \frac{1}{N}\sqrt{N} = \frac{1}{\sqrt{N}}, \tag{4.3}$$

which explains the nonzero values of M^z in the “disordered" phase for small systems in Figure 4.1. However the largest systems we can treat in our exact diagonalization simulations have $N \approx 16$ (Figure 4.3) if only the ground state energy and wave functions are calculated. For other observables such as M^z and M^x the limit on the system size is even lower. For larger systems we use the DMRG

method within which the Lanczos code is called to diagonalize the effective Hamiltonian at each step.

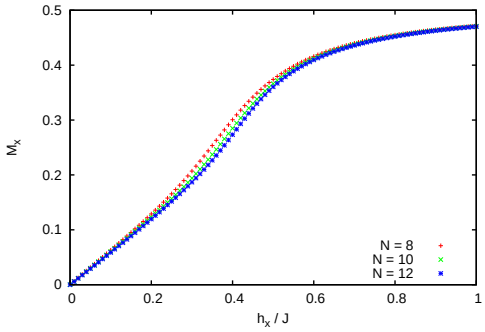

Figure 4.2: M^x for the ferromagnetic transverse field Ising model as a function of h_x/J for different values of system sizes N calculated by our Lanczos simulation.

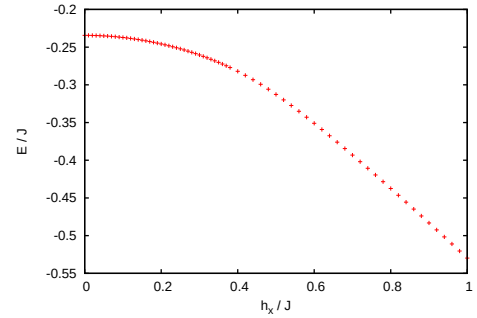

Figure 4.3: The ground state energy per site for a 16-site ferromagnetic transverse field Ising model as a function of h_x/J calculated by our Lanczos simulation

4.2 Density Matrix Renormalization Group

To simulate larger system sizes we implemented the density matrix renormalization group algorithm. The phase transition is more clearly observed in the DMRG results since the systems to be treated are larger than when we used ED, and hence the order parameter, M^z in ferromagnetic

systems and the staggered magnetization N^z in antiferromagnetic systems, have very small values in the disordered phase.

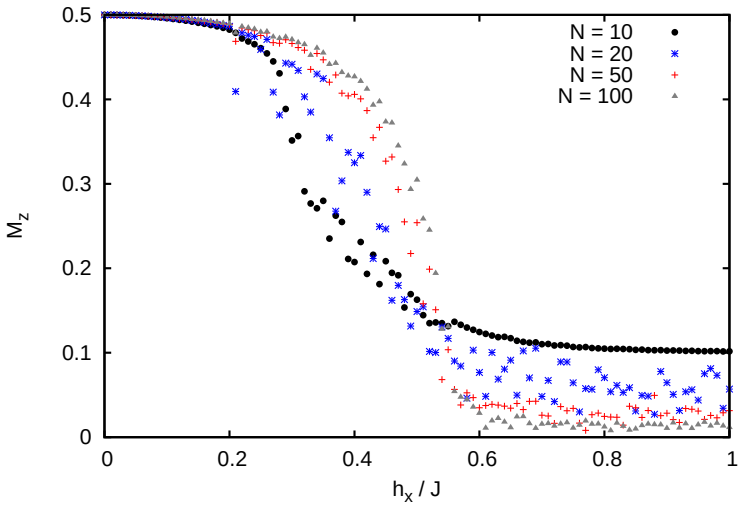

Figure 4.4: M^z in the ferromagnetic Ising chain in a transverse field with N sites and 256 states kept in the density matrix truncation, obtained from the infinite-system DMRG calculations. To have a more fair comparison between the results for different N we need to keep more states for larger systems, but the maximum number of states one can keep is restricted due to the limitations on the memory.

Ground State Properties

The result of the infinite-system DMRG simulation for the ground state magnetization M^z in the TFIM is shown in Figure 4.4. The infinite-system DMRG results can be improved by keeping more states in the truncation procedure (Sec. 3.3.2). Our simulation results confirm a better convergence (especially around the critical point, $h_x/J = 0.5$) for a larger number of states kept (Figure 4.5).

However, to increase the accuracy and avoid the problems mentioned in Sec. 3.3.2, it is desirable to carry on several finite-system sweeps along the system after the desired length is achieved with the infinite system algorithm [27]. We have observed that by taking only a few sweeps, in spite of keeping a very small number of states in the DMRG truncation, we can obtain more reliable results (Figure 4.6).

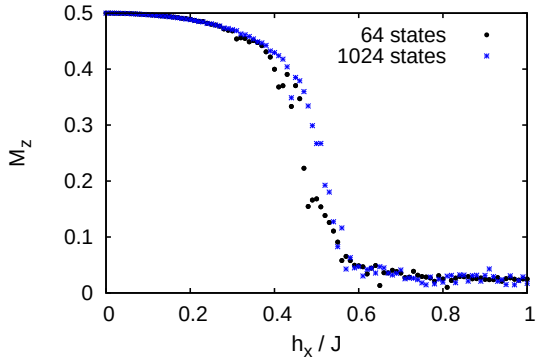

Figure 4.5: Comparison of M^z in a 50-site ferromagnetic Ising chain in a transverse field for different values of the number of states kept in the infinite-system DMRG algorithm.

Higher accuracy with the DMRG method can then be achieved by tuning the control parameters such as the number of states kept, the number of sweeps along the system, and iterations in the ED part of the algorithm towards a better convergence.

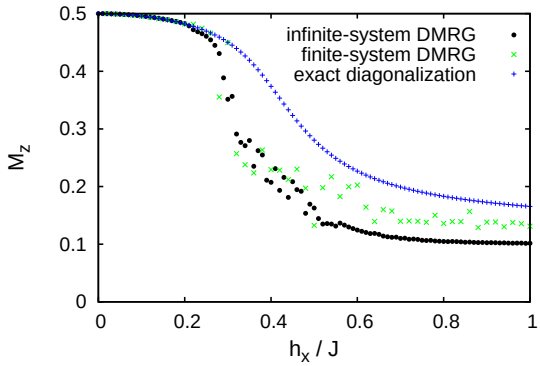

Figure 4.6: M^z in a 10-site ferromagnetic Ising chain in a transverse field. Comparison of the ED, inifinite-system DMRG, and finite-system DMRG with 10 sweeps along the system and 256 states kept.

In antiferromagnetic systems, the maximum staggered magnetization, $N^z = 0.5$, corresponds to the state with all the spins aligned antiparallel to their nearest neighbour, indicating the “antiferromagnetic" phase (Figure 4.7). The phase transition from the gapped to the gapless phase, shown

in Sec. 2.1, does not depend on the sign of J which means that the value for the critical field h_x^c in antiferromagnetic and ferromagnetic systems is the same.

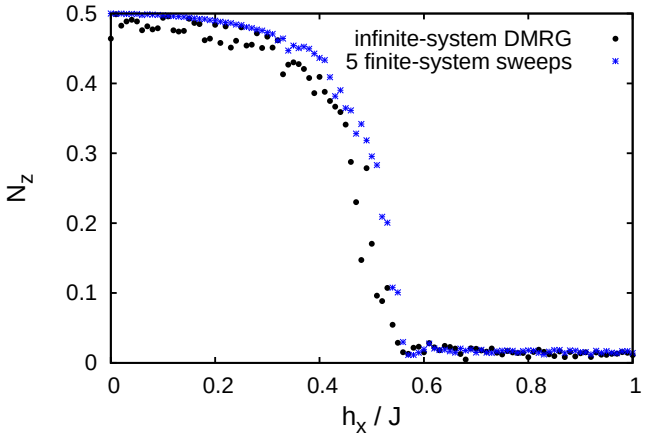

Figure 4.7: The staggered magnetization, N^z as a function of h_x, in a 100-site antiferromagnetic Ising chain in a transverse field, keeping 256 states.

Now let's consider an Ising chain in the presence of both transverse and longitudinal fields:

$$H = J\sum_{i=1}^{N} {S_i}^z {S_{i+1}}^z + h_x \sum_{i=1}^{N} {S_i}^x + h_z \sum_{i=1}^{N} {S_i}^z, \tag{4.4}$$

This model was discussed in Sec. 2.2. The phase diagram revealing the antiferromagnetic and paramagnetic phases for the ground state of model 4.4 obtained from our simulations is shown in Figure 4.8, which is in very good agreement with Ref. [25] (see Figure 2.1).

4.3 Out of Equilibrium Dynamics

Our DMRG simulations so far have provided reasonable results and give us the confidence to extend our work to the time dependent regime. In this section we present our tDMRG results where we use time step targeting (Sec. 3.3.4) for the simulation of the time evolution of our system after a quench in a system parameter. We measure time in units of $\hbar/J$, and this should be understood in all figures in this chapter.

Our calculations take the form of making a quench in the transverse or longitudinal field and then studying the response of the order parameter to this change.

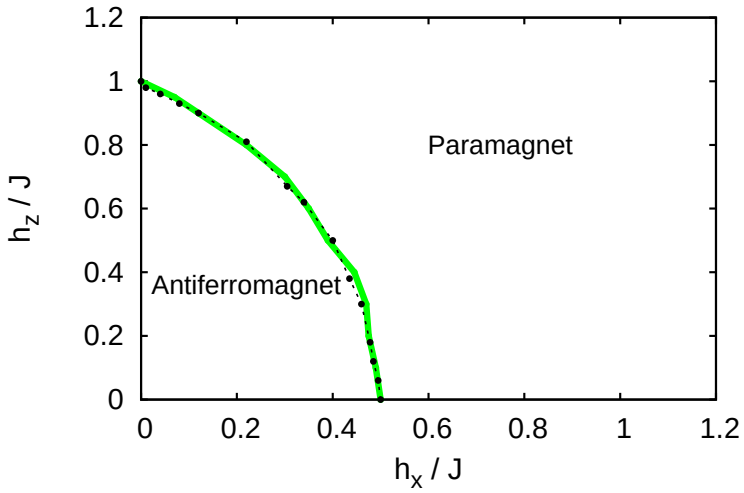

Figure 4.8: The ground state phase diagram of an antiferromagnetic system in the presence of both longitudinal and transverse fields (model 4.4). The results are obtained from a DMRG simulation of a 50-site system, keeping 256 states. The dashed line shows the results obtained by Ovchinnikov *et al.* [25] as discussed in Sec. 2.2

However, as discussed earlier the results of simulations for tDMRG algorithms becomes inaccurate with increasing time (Sec. 3.3.4). Hence, we need to verify the range of the time within which our results are reliable before taking data. A benchmark for the reliability of the results at time t is the fidelity, $F = |\langle\psi_0|\psi_t\rangle|$, where ψ_t (ψ_0) is the wave function at time t (zero).

It is easier to monitor the infidelity, $I = 1 - F$, which is shown in Figure 4.9 for a transverse field Ising chain with $h_x/J = 0.2$. In the calculation with $h_x/J = 0.2$, there is no change in H (unlike a quench) and so if we were able to get a good enough initial state ψ_0, i.e. an eigenstate of H, we should have $I = 0$. Therefore we need to consider the two cases i) when ψ_0 is an eigenstate of H, and ii) when ψ_0 is not an eigenstate of H.

The state of the system at time t is obtained by acting the time evolution operator, $U = e^{-\frac{iHt}{\hbar}}$, with the initial state:

$$|\psi_t\rangle = \exp\left[\frac{-iHt}{\hbar}\right]|\psi_0\rangle. \tag{4.5}$$

The infidelity at time t for case i) can then be written as

$$I = 1 - \left| \langle \psi_0 | \exp\left[\frac{-iHt}{\hbar}\right] |\psi_0\rangle \right| = 1 - \left| \exp\left[\frac{-iE_0 t}{\hbar}\right] \right| = 0, \tag{4.6}$$

hence zero at all times. However, if the initial state is not an eigenstate of H, the infidelity does not remain zero. Consider the situation where the time evolution procedure starts from a wave function that is slightly different from the ground state of the initial Hamiltonian

$$|\psi\rangle = \alpha|\psi_0\rangle + \beta|\psi_i\rangle, \tag{4.7}$$

where $\langle\psi_0|\psi_i\rangle = 0$. In this case the infidelity in short times is given by

$$\begin{aligned} I &= 1 - \left| \{\alpha^* \langle\psi_0| + \beta^* \langle\psi_i|\} \exp\left[\tfrac{-iHt}{\hbar}\right] \{\alpha|\psi_0\rangle + \beta|\psi_i\rangle\} \right| \\ &= 1 - \left| |\alpha|^2 \exp\left[\tfrac{-iE_0 t}{\hbar}\right] + |\beta|^2 \langle\psi_i| \exp\left[\tfrac{-iHt}{\hbar}\right] |\psi_i\rangle \right| \\ &\simeq 1 - \left| |\alpha|^2 \exp\left[\tfrac{-iE_0 t}{\hbar}\right] + |\beta|^2 \left[1 - \tfrac{it}{\hbar}\langle\psi_i|H|\psi_i\rangle\right] \right| + O(t^2) \\ &\simeq 1 - |\alpha|^2 - |\beta|^2 + O(t^2). \end{aligned} \tag{4.8}$$

The above expression suggests that in case i), where $\alpha = 1$ and $\beta = 0$, $I = 0$. Otherwise I grows linearly in time for small enough t.

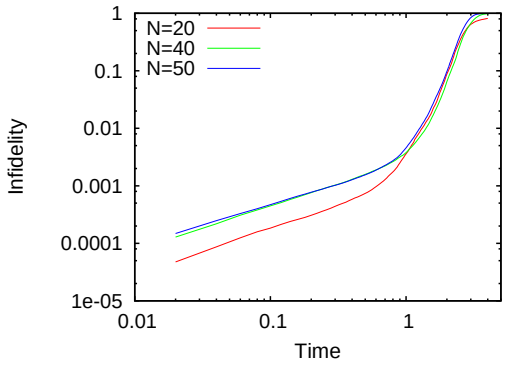

Figure 4.9: The infidelity as a function of time for ferromagnetic Ising chain in a transverse field at $h_x/J = 0.2$, keeping 1024 states.

The origin of the presence of other states in the initial wavefunction is the truncation of the

Hilbert space. As a result of truncation, the wave function found at the end of the DMRG sweeps (before the time evolution) does not necessarily represent the ground state of the system, but it may also include a superposition of some of the low-lying states which may have small overlap with the ground state. The error arising from approximation of the wavefunction then leads to a nonzero infidelity which grows rapidly in time as the truncation error dominates the total error (see Sec. 3.3.4).

Current efficient classical algorithms for computing dynamics of quantum systems are yet less developed than for computing static properties. In a recent experiment in cold atoms it has been shown that the experimental dynamics run for longer than present algorithms such as tDMRG [65]. Hence the growth of the infidelity in tDMRG calculations is one of the main challenges in the field. For a fixed number of states kept (1024 states in Figure 4.9), the wave function in the truncated Hilbert space is a better approximation to the actual ground state for smaller system sizes. When the number of states kept is much smaller than 2^N the low-lying excitations have larger contributions in the approximation to the ground state wave function which leads to larger deviations during the time evolution.

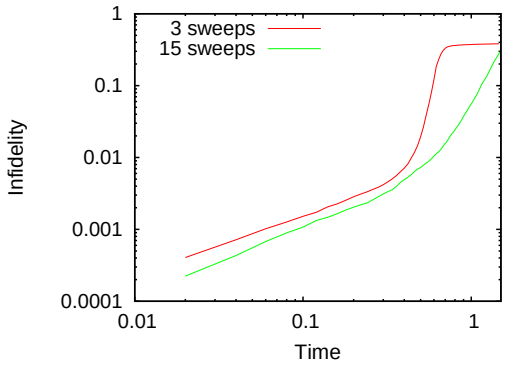

Figure 4.10: The infidelity as a function of time for a 20-site ferromagnetic Ising chain in a transverse field at $h_x/J = 0.2$, keeping 1024 states, with different values of DMRG sweeps completed before the beginning of the time evolution.

The infidelity can then be decreased by keeping a larger number of states or by doing more finite-system DMRG sweeps before starting the time evolution, so that the initial wave function becomes a better approximation to the actual ground state. We use a combination of these two solutions to improve the results for different systems. The effect of the latter on the improvement of

the results is shown in Figure 4.10.

From similar graphs such as Figures 4.9 and 4.10, we chose appropriate values for the control parameters like the number of states and sweeps, for every N and run the simulation for them within the valid time range. We now present our results for the out of equilibrium dynamics in a transverse field Ising chain.

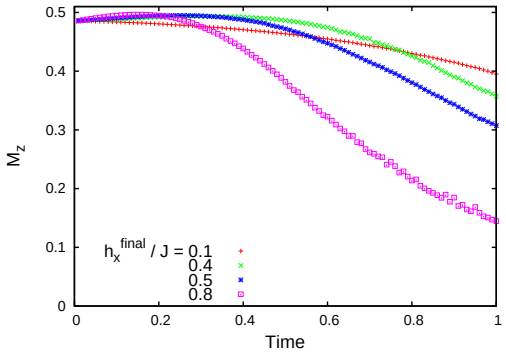

Figure 4.11: M^z in a 20-site ferromagnetic Ising chain in a transverse field after a quench from $h_x/J = 0.2$ to different values of h_x. There is no ordering in quenches from larger to smaller transverse field since there is no bath to allow the system to exchange energy and go to the ground state of the Hamiltonian that it is evolving with.

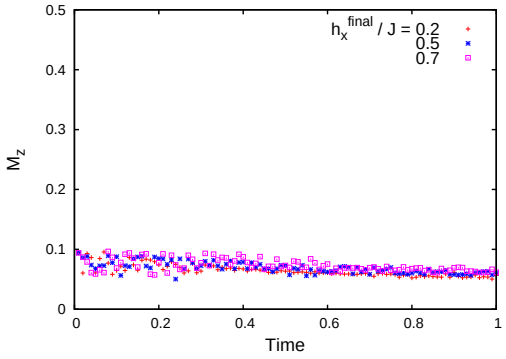

Figure 4.12: M^z in a 20-site ferromagnetic Ising chain in a transverse field after a quench from $h_x/J = 0.8$ to different values of h_x

Figure 4.11 shows how the magnetization, M^z, behaves after a quench in the transverse field

from an initial value within the ferromagnetic phase ($h_x^0/J = 0.2$) to different final values h_x. The decay, observed for all values of h_x, was analytically predicted in Ref. [30]. The analytical expression for $M^z_{(t)}$ is derived for the asymptotic late-time regime which is not accessible by tDMRG, However for a qualitative comparison of our simulation results with the analytical predictions, see Figure 1.6. For quenches starting from the disordered phase ($h_x/J > 0.5$) the magnetization is expected to be zero at all times since the Z_2 symmetry (given by Eq. 2.2) remains unbroken [30]. This is in agreement with our results (Figure 4.12).

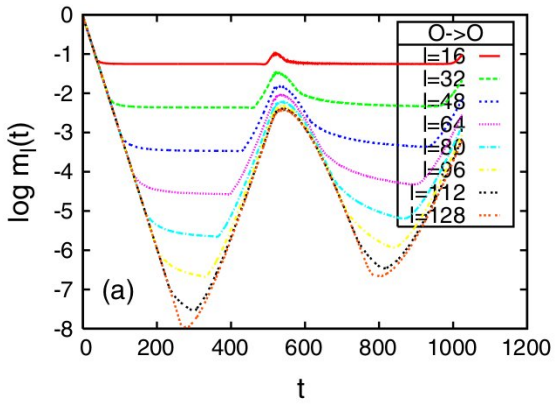

Figure 4.13: Relaxation of the local magnetization in a $L = 256$ chain after a quench from $h_x/J = 0$ to $h_x/J = 0.25$ [32]. The recurrence in $m_l(t)$ occurs at a time $T = L/v$, where $v = v(h, h_0)$ is the speed of the quasiparticles.

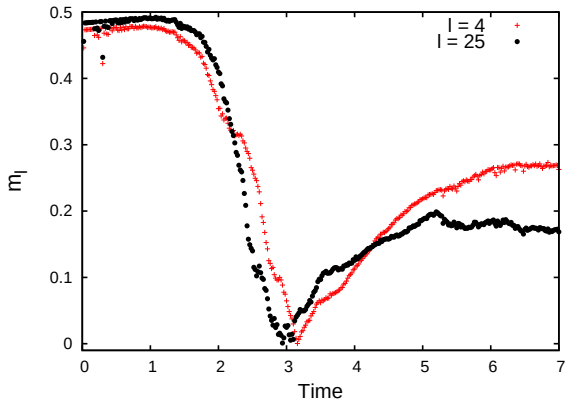

Figure 4.14: Local magnetization at site l as a function of time in a 50-site ferromagnetic transverse field Ising chain after a quench from $h_x/J = 0.2$ to $h_x/J = 0.3$.

The time evolution of local magnetization, $m_l(t) = \langle\psi_t|S_l^z|\psi_t\rangle$, after a quench from h_0 to h in the TFIM, was studied analytically in Ref. [32]. The two “decay" and “reconstruction" regimes (Figure 4.13) introduced in the nonequilibrium relaxation of the magnetization profiles agrees with our tDMRG simulations (Figure 4.14). The reconstruction of the local observable $m_l(t)$ corresponds to the case when the quasiparticles, which are emitted at $t = 0$ and arrive at a reference point l in time t, originate from nearby regions in space. In the relaxation regime only incoherent quasiparticles pass the reference point. However, this agreement is qualitative and one should not regard all the details as quantitatively accurate since the time range illustrated in this plot is well beyond the reliable range of our DMRG simulations.

In an antiferromagnetic Ising chain in the presence of both longitudinal and transverse fields (model 4.4) we carry out quenches between different regions in the phase diagram (Figure 4.15). While the possibility of experimentally investigating quenches of this sort has been recently provided in cold atom systems [16, 66], yet there has not been theoretical studies on what we consider in this work.

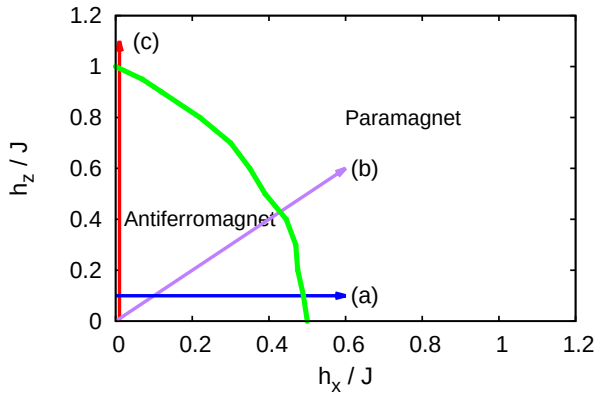

Figure 4.15: We consider quenches along the schematic lines shown in the phase diagram.

The response of the order parameter to quenches within the ordered phase, from the ordered to disordered phase or vice versa, are shown in Figures 4.16, 4.17, and 4.18.

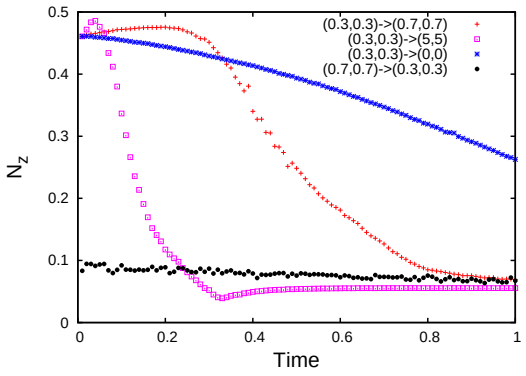

Figure 4.16: Time evolution of the staggered magnetization N_z after a quench of the fields from $(h_z^0/J, h_x^0/J)$ to $(h_z^{\text{final}}/J, h_x^{\text{final}}/J)$, corresponding to a quench of type (b) in Fig. 4.15, in a 20-site chain with 1024 states kept.

According to our results in quenches of types a, b, and c, starting from the ordered phase the antiferromagnetic order decays for any final values of the fields. The decay is faster for larger quenches i.e. when h_x and h_z are further from the critical line. In quenches starting from the disordered phase the order parameter N_z remains zero for all times.

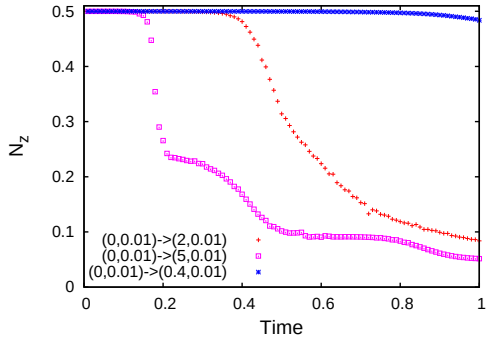

Figure 4.17: Time evolution of the staggered magnetization N_z after a quench of the fields from $(h_z^0/J, h_x^0/J)$ to $(h_z^{\text{final}}/J, h_x^{\text{final}}/J)$, corresponding to a quench of type (c) in Fig. 4.15, in a 20-site chain with 1024 states kept.

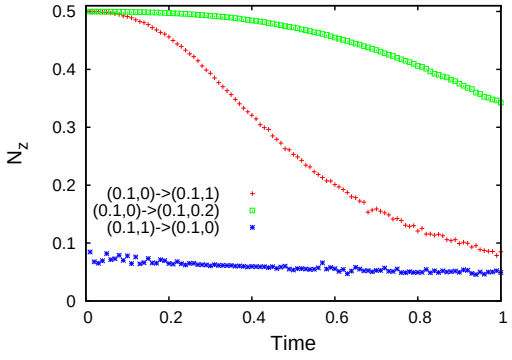

Figure 4.18: Time evolution of the staggered magnetization N_z after a quench of the fields from $(h_z^0/J, h_x^0/J)$ to $(h_z^{\text{final}}/J, h_x^{\text{final}}/J)$, corresponding to a quench of type (a) in Fig. 4.15, in a 20-site chain with 1024 states kept.

Now it is worth taking a more precise look at the quenches close to the multicritical point at $(h_z, h_x) = (1, 0)$ since the neighbourhood of this point is the region in which the Bose-Hubbard model was mapped onto the antiferromagnetic Ising spin chain in the cold atom experiment in Ref. [16]. Their approximate experimental path lies along the red arrow in Figure 4.15. Although the transition from the paramagnetic to antiferromagnetic phase was claimed to occur adiabatically in the experiment, the possibility of simulating out of equilibrium processes in cold atoms [17, 65, 66] motivates us to study the out of equilibrium dynamics of the system nearby this region.

We study the behaviour of N_z after quenches close to the multicritical point (Figure 4.19), extracting a time scale t^* to characterize the dynamics after the quench. Our results suggest a faster relaxation of the order parameter for quenches further from the critical line, similar to what we observed in the quenches of types a, b, and c.

We define the characteristic time, t^* as the time in which the staggered magnetization drops to $2/e$ of its initial value after quenches of type (c) (in Figure 4.15) from the ordered to disordered phase. The results, exhibited in Figure 4.20, suggest that in an antiferromagnetic Ising chain given by Eq. 4.4, the characteristic time for the decay of the order parameter after a quench from the ordered to disordered phase, exponentially decreases by moving away from the multicritical point.

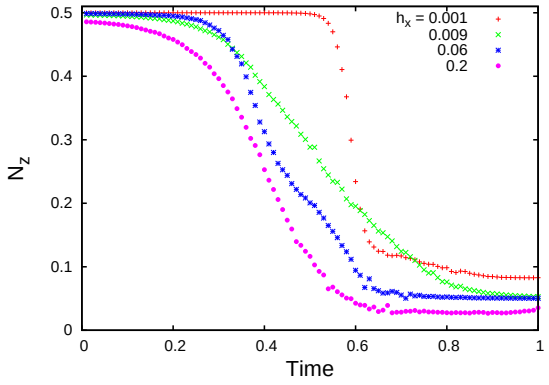

Figure 4.19: Time evolution of the staggered magnetization N_z after a quench in the fields from $(h_z^0/J, h_x/J)$ to $(h_z^{\text{final}}/J, h_x/J)$ close to the multicritical point in a 20-site chain with 1024 states kept.

However, the goal for investigating criticality through studying the behaviour of t^* is not fulfilled since we are limited by the growth of infidelity in the timescale we can simulate.

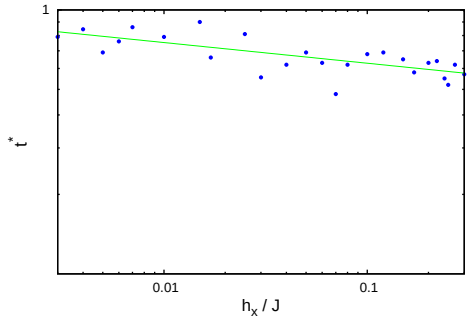

Figure 4.20: The time in which N_z drops to $2/e$ of its initial value after the quenches from $(h_z^0 = 0, h_x)$ to $(h_z^{\text{final}} = 2, h_x)$ for different values of h_x for 20-site chain with 1024 states. In this plot t^* decreases as $t^* \sim h_x^{-0.078}$. The fit to the data has been found through the least-squares Marquardt-Levenberg algorithm using Gnuplot, with an error of 0.015 in calculating the slope of the fitted line.

4.4 Summary

In this chapter we studied the ground state phase diagram and out of equilibrium dynamics of Ising spin chains in the presence of transverse and longitudinal magnetic fields. The presented results from the exact diagonalization and DMRG calculations exhibit the previously studied [8, 25] quantum phase transition at the critical values of the fields. Plots of the order parameters in different systems imply that DMRG results can be enhanced by tuning the control parameters such as the kept number of states and the number of sweeps in a finite-system algorithm. The results for the DMRG simulations provide evidence that our code is reliable and capable of extending to out of equilibrium regime.

Applying time evolution methods in DMRG is restricted to short times due to the exponential growth of the truncation error in time. On one hand, the greater the system, the larger number of states need to be kept to keep the truncation error small in a specific amount of time. On the other hand, treating smaller systems causes our results to suffer from some finite size effects. This limits the system sizes we can treat by tDMRG with a fixed number of states kept. The time range within which our results are reliable is found by investigating the infidelity as a function of time. The improvement of the fidelity with the number of finite-system sweeps before the time evolution procedure is further illustrated.

For observing the out of equilibrium behaviour of different systems, we performed quenches of the fields at $t = 0$ and observed the response of the order parameters within the valid time range. In ferromagnetic Ising chains in a transverse field, M^z decays in quenches starting in the ferromagnetic phase and remains zero for quenches starting in the paramagnetic phase. Antiferromagnetic chains in the presence of mixed fields have a richer phase diagram and are studied through quenches of different types. In the cases studied here, the order parameter N^z, exhibits a decay in quenches starting in the ordered phase and persistent low-amplitude oscillations (Figure 4.16) around zero in quenches starting in the disordered phase. Investigating quenches in the vicinity of the multicritical point at $h_x = 0$, $h_z = 1$, we find indications of a very weak power law dependence of the relaxation time for the order parameter as a function of h_x^{initial}.

Chapter 5

Conclusion

The quantum Ising chain with antiferromagnetic interactions and both transverse and longitudinal magnetic fields has been studied much less extensively than the solvable TFIM. Here we studied the out of equilibrium dynamics of this model under quantum quenches, which had not previously been studied. This is particularly timely given recent cold atom experiments that realize this model and allow for the study of such dynamics [16, 66]. In this thesis we have implemented exact diagonalization and density matrix renormalization group (DMRG) techniques to study numerically the ground state properties of this model. We have obtained the ground state energy and wave function, and illustrated the phase transition from a gapped to a gapless phase which happens at the critical values of the fields as derived in previous studies of the model [25].

We then developed a time dependent DMRG code to study out of equilibrium dynamics in the system. We have investigated the evolution of the order parameters after different types of quenches of the magnetic fields for a variety of initial conditions. Our results in the ferromagnetic systems are in qualitative agreement with analytical predictions [19, 31, 32]. In antiferromagnetic chains the results from our tDMRG simulations suggest a decay of the order parameter in quenches starting from the ordered phase. The limiting factors for the accuracy of our calculations were finite size effects and the growth of infidelity with time.

The t-DMRG code that has been developed here has been written so as to be as flexible as possible for future applications. In particular, by using time step targeting for time evolution, we allow for the possibility of treating spin chains with longer range interactions than just nearest neighbours. The transverse field Ising chain with appropriate three spin interactions is found to exhibit topologically non-trivial phases with Majorana fermion states [67]. Future work could involve studying

the out of equilibrium dynamics in quenches between these topologically non-trivial ground states. Given the rapid pace of experimental developments, such models may be possible to be simulated in the near future.

Another future direction involves the study of two-point correlation functions of the form $\langle\psi|O_l O_m|\psi\rangle$, which can be calculated using DMRG as discussed in Sec. 3.3.3.1. O_l and O_m might be spin operators acting on different sites at the same time, or operators acting on the same site at different times (in a tDMRG simulation). Correlations between different spins or the autocorrelation of individual spins are interesting quantities to look at in investigating the dynamics of a many-body system and can provide helpful information about the equilibration of the system on a microscopic level.

Bibliography

[1] W. Gerlach and O. Stern, Z. Phys. A **9**, 353 (1922).

[2] G. E. Uhlenbeck and S. Goudsmit, Nature **117**, 264 (1926).

[3] E. Ising, Z. Phys. A **31**, 253 (1925).

[4] L. Onsager, Phys. Rev. **65**, 117 (1944).

[5] H. Bethe, Z. Phys. **71**, 205 (1931).

[6] L. Hulthen, Arkiv Mat. Astron. Fysik **26A**, 11 (1938).

[7] E. H. Lieb and F. Wu, Phy. Rev. Lett. **20**, 1445 (1968).

[8] E. Lieb, T. Schultz, and D. Mattis, Ann. Phys. **16**, 407 (1961).

[9] P. G. de Gennes, Sol. State Commun. **1**, 132 (1963).

[10] I. Bloch, Nature **453**, 1016 (2008).

[11] A. E. Feiguin, A. Avella, and F. Mancini, in *Strongly Correlated Systems*. Springer Series in Solid-State Sciences, Vol. **176**-Verlag Berlin Heidelberg (2013).

[12] O. Morsch and M. Oberthaler, Rev. Mod. Phys. **78**, 179 (2006).

[13] I. Bloch, J. Dalibard, and W. Zwerger, Rev. Mod. Phys. **80**, 885 (2008).

[14] D. Jaksch, C. Bruder, J. I. Cirac, C. W. Gardiner, and P. Zoller, Phys. Rev. Lett. **81**, 3108 (1998).

[15] M. Greiner, O. Mandel, T. Esslinger, T. W. Hänsch, and I. Bloch, Nature **415**, 39 (2002).

[16] J. Simon, W. S. Bakr, R. Ma, M. E. Tai, P. M. Preiss, and M. Greiner, Nature **472**, 307 (2011).

[17] T. Kinoshita, T. Wenger, and D. S. Weiss, Nature **440**, 900 (2006).

[18] S. Sachdev and A. Young, Phys. Rev. Lett. **78**, 2220 (1997).

[19] K. Sengupta, S. Powell, and S. Sachdev, Phys. Rev. A **69**, 053616 (2004).

[20] O. Viehmann, J. V. Delft, and F. Marquardt, Phys. Rev. Lett. **110**, 030601 (2013).

[21] Y. L. Wang and B. R. Cooper, Phys. Rev. **172**, 539 (1968).

[22] P. Pfeuty and R. Elliott, J. Phys. C **4**, 2370 (1971).

[23] D. Bitko, T. Rosenbaum, and G. Aeppli, Phys. Rev. Lett. **77**, 940 (1996).

[24] R. Coldea, D. Tennant, E. Wheeler, E. Wawrzynska, D. Prabhakaran, M. Telling, K. Habicht, P. Smeibidl, and K. Kiefer, Science **327**, 177 (2010).

[25] A. A. Ovchinnikov, D. V. Dmitriev, V. Y. Krivnov, and V. O. Cheranovskii, Phys. Rev. B **68**, 214406 (2003).

[26] H. C. Fogedby, J. Phys. C **11**, 2801 (1978).

[27] R. M. Noack and S. R. White, in *Density-Matrix Renormalization*. Springer (1999).

[28] J. W. Britton, B. C. Sawyer, A. C. Keith, C. J. Wang, J. K. Freericks, H. Uys, M. J. Biercuk, and J. J. Bollinger, Nature **484**, 489 (2012).

[29] K. Kim, M. S. Chang, S. Korenblit, R. Islam, E. E. Edwards, J. K. Freericks, G. D. Lin, L. M. Duan, and C. Monroe, Nature **465**, 590 (2010).

[30] P. Calabrese, F. H. Essler, and M. Fagotti, J. Stat. Mech. **2012**, 07016 (2012).

[31] P. Calabrese, F. H. Essler, and M. Fagotti, Phys. Rev. Lett. **106**, 227203 (2011).

[32] F. Iglói and H. Rieger, Phys. Rev. Lett. **106**, 035701 (2011).

[33] F. Iglói and H. Rieger, Phys. Rev. Lett. **85**, 3233 (2000).

[34] A. Yu Kitaev, Phys. Usp. **44**, 131 (2001).

[35] M. Kenzelmann, R. Coldea, D. A. Tennant, D. Visser, M. Hofmann, P. Smeibidl, and Z. Tylczynski, Phys. Rev. B **65**, 144432 (2002).

[36] N. W. Ashcroft and N. D. Mermin, *Solid State Physics*. Brooks Cole: New York (1976).

[37] E. Dagotto, Rev. Mod. Phys. **66**, 763 (1994).

[38] C. Lanczos, *An iteration method for the solution of the eigenvalue problem of linear differential and integral operators*. U.S. Governm. Press Office (1950).

[39] D. Calvetti, L. Reichel, and D. C. Sorensen, Electronic Transactions on Numerical Analysis **2**, 21 (1994).

[40] K. G. Wilson, Rev. Mod. Phys. **47**, 773 (1975).

[41] U. Schollwöck, Rev. Mod. Phys. **77**, 259 (2005).

[42] S. R. White and R. M. Noack, Phys. Rev. Lett. **68**, 3487 (1992).

[43] S. R. White, Phys. Rev. Lett. **69**, 2863 (1992).

[44] S. R. White and R. L. Martin, J. Chem. Phys. **110**, 4127 (1999).

[45] J. Dukelsky and G. Sierra, Phys. Rev. Lett. **83**, 172 (1999).

[46] S. R. White and D. A. Huse, Phys. Rev. B **48**, 3844 (1993).

[47] S. Liang and H. Pang, Phys. Rev. B **49**, 9214 (1994).

[48] S. Moukouri and L. G. Caron, Phys. Rev. B **67**, 092405 (2003).

[49] C. D. E. Boschi and F. Ortolani, Eur. Phys. J. B **41**, 503 (2004).

[50] H. Fehske, R. Schneider, and A. Weiße, *Computational Many-particle Physics*. Springer (2008).

[51] A. E. Feiguin and S. R. White, Phys. Rev. B **72**, 020404 (2005).

[52] S. Östlund and S. Rommer, Phys. Rev. Lett. **75**, 3537 (1995).

[53] S. R. White, Phys. Rev. Lett. **77**, 3633 (1996).

[54] G. Alvarez, L. da Silva, E. Ponce, and E. Dagotto, Phys. Rev. E **84**, 056706 (2011).

[55] J. Grotendorst, D. Marx, and A. Muramatsu, *Quantum Simulations of Complex Many-Body Systems: From Theory to Algorithms - Lecture Notes*, J. Neumann Inst. Comp. Forschungszentrum, Jülich (2002).

[56] C. H. Mak, Phys. Rev. Lett., **68**, 899 (1992).

[57] R. Egger and C. H. Mak, Phys. Rev. B **50**, 15210 1994.

[58] S. R. Manmana, A. Muramatsu, and R. M. Noack, AIP Conf. Proc. 789 (2004).

[59] H. G. Luo, T. Xiang, and X. Wang, Phys. Rev. Lett. **91**, 49701 (2003).

[60] M. A. Cazalilla and J. B. Marston, Phys. Rev. Lett. **88**, 256403 (2002).

[61] G. Vidal, Phys. Rev. Lett. **91**, 147902 (2003).

[62] S. R. White and A. E. Feiguin, Phys. Rev. Lett. **93**, 076401 (2004).

[63] I. Peschel and V. Eisler, J. Phys. A **42**, 504003 (2009).

[64] P. Calabrese and J. Cardy, J. Stat. Mech. **2007**, 10004 (2007).

[65] S. Trotzky, Y. A. Chen, A. Flesch, I. P. McCulloch, U. Schollwöck, J. Eisert, and I. Bloch, Nature Phys., **8**, 325 (2012).

[66] F. Meinert, M. J. Mark, E. Kirilov, K. Lauber, P. Weinmann, A. J. Daley, and H. C. Nägerl, Phys. Rev. Lett. **111**, 053003 (2013).

[67] Y. Niu, S. B. Chung, C. H. Hsu, I. Mandal, S. Raghu, and S. Chakravarty, Phys. Rev. B **85**, 035110 (2012).